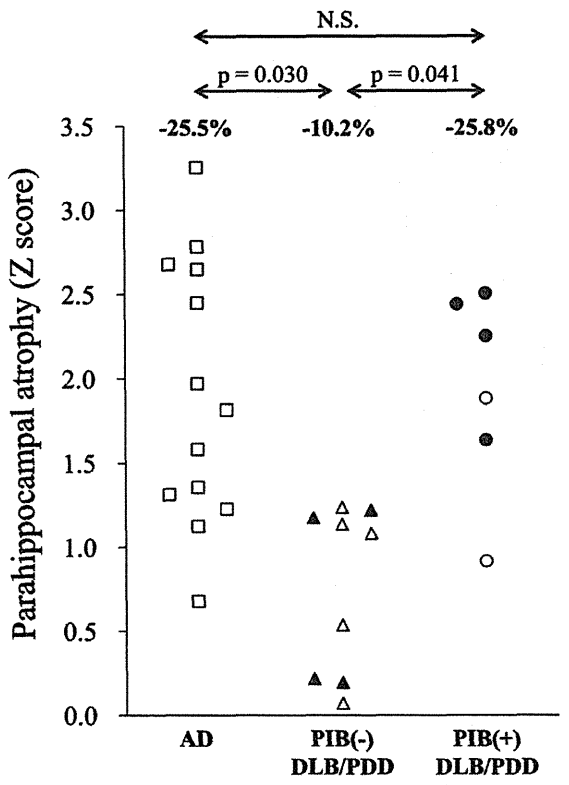

FIG. 3. Z-scores of parahippocampal atrophy in three groups. Scatter plot of individual Z-scores of GMV reduction in the parahippocampus, compared to those of the healthy control group. Filled circles and triangles indicate DLB, whereas open circles and triangles indicate PDD.

coexistent AD-type pathology, such as Aβ and tau, whereas both cortical LBs and AD-type pathology are rare in PD without dementia.[2] Aβ pathology would be linked with other pathological changes, such as tau and cortical LBs, which may be associated with dementia and cortical atrophy in DLB/PDD patients.

A pathological study reported that a high cortical Aβ score along with an older age at onset were associated with a shorter time-to-dementia period in PDD.[25] Rowe et al. reported that cortical PIB binding was correlated inversely with the interval from onset of cognitive impairment to diagnosis in DLB.[26] Longitudinal studies in DLB/PDD patients will be required to elucidate whether Aβ deposition accelerates the progression of dementia and brain atrophy and whether alpha-synuclein accelerates Aβ deposition in the brain.

Mean cortical PIB binding also did not correlate with voxel-by-voxel GMV in DLB/PDD patients in the present study. Chételat et al. found an association between cortical atrophy and Aβ deposition at subjective cognitive impairment, but not in mild cognitive impairment (MCI) and AD.[27] This finding suggests that Aβ deposition is likely to reach a plateau in the very early disease process of AD, and there are downstream drivers of progressive atrophy from the MCI stage. The lack of correlation between PIB uptake and cortical atrophy in DLB/PD could also be attributed to such time courses of Aβ deposition and cortical atrophy.

In pathological studies, most DLB patients showed cortical Aβ burdens.[28] Ballard et al. reported that 25 of 29 DLB patients (87%) and 12 of 28 PDD patients (43%) had moderate or abundant cortical amyloid plaques measured using the Consortium to Establish a Registry for Alzheimer's Disease protocol,[29] 2 of 29 DLB patients (7%) and 6 of 28 PDD patients (21%) had scarce cortical amyloid plaques, and 2 of 29 DLB patients (7%) and 10 of 28 PDD patients (36%) had no cortical amyloid plaques.[28] Aβ plaques appear to be more frequent in postmortem DLB/PDD brains in pathological studies than in *in vivo* PET studies, but this could be explained by the fact that most postmortem brains were obtained at the terminal stage of DLB/PDD.

The distribution of cortical atrophy observed in 6 PIB(+) DLB/PDD patients in our study was quite similar to that in AD patients. Perhaps it may be a more-interesting finding in this study that there was no striking gray-matter atrophy, despite the presence of

TABLE 2. GMV reduction normalized by total intracranial volumes, compared to controls

	DLB/PDD			
	PIB(−)	PIB(+)	AD	Note
Frontal	1.65 ± 1.54	3.04 ± 1.52[b]	2.60 ± 1.40[b]	
Sensorimotor	0.85 ± 1.15	1.42 ± 0.84	1.22 ± 1.05	
Parietal	1.34 ± 1.22	2.28 ± 0.40[b]	2.08 ± 1.30[a]	
Striatum	1.22 ± 1.30	2.23 ± 1.60[a]	2.14 ± 2.06[a]	
Occipital	1.18 ± 0.86	1.70 ± 1.02[a]	1.94 ± 1.04[b]	
Lateral temporal	1.40 ± 0.93	2.81 ± 1.26[b]	3.22 ± 1.24[b]	
Parahippocampal area	0.76 ± 0.50	1.94 ± 0.60[b]	1.91 ± 0.78[b]	PIB(−) < AD, PIB(−) < PIB(+)[a]
Hippocampus	0.66 ± 1.07	1.82 ± 0.94[a]	2.21 ± 0.96[b]	PIB(−) < AD[a]
Amygdala	0.83 ± 1.43	2.67 ± 1.51[a]	3.71 ± 1.59[b]	PIB(−) < AD[b]

GMV reduction, compared to controls, adjusted by each intracranial volume, is expressed by Z-score, and values are listed as mean ± SD.
[a]$P < 0.05$.
[b]$P < 0.01$ (rank ANCOVA, adjusting for differences in age, followed by Bonferroni's correction).

dementia, in PIB(−) DLB/PDD patients. Graff-Radford et al. reported that patients with DLB, but without the imaging features of coexistent AD-related pathology, such as parahippocampal atrophy and PIB(+), were more likely to cognitively improve with acetylcholinesterase inhibitor treatment.[30] These findings would suggest a predominant subcortical mechanism, such as cholinergic dysfunction, underlying dementia in beta-amyloid-negative DLB patients.

Limitations of the study are the small number of DLB/PDD patients and the lack of the investigation about cholinergic function. Therefore, further studies are needed to confirm the mechanism of dementia, especially in beta-amyloid-negative DLB patients.

Conclusions

In conclusion, our results suggest that Aβ deposition is associated with AD-like atrophy in DLB/PDD. Anti-amyloid therapy for AD is in progress, with promising evidence for the reduction of Aβ. Early intervention against Aβ may prevent or delay AD-like atrophy in patients with DLB/PDD with Aβ deposition. ■

Acknowledgments: The authors thank all patients and volunteers for their participation in the study as well as all investigators and their site staff for their contributions.

References

1. Lippa CF, Duda JE, Grossman M, et al.; the DLB/PDD Working Group. DLB and PDD boundary issues: diagnosis, treatment, molecular pathology, and biomarkers. Neurology 2007;68:812–819.
2. Tsuboi Y, Dickson DW. Dementia with Lewy bodies and Parkinson's disease with dementia: are they different? Parkinsonism Relat Disord 2005;11(Suppl 1):S47–S51.
3. Klunk WE, Engler H, Nordberg A, et al. Imaging brain amyloid in Alzheimer's disease with Pittsburgh Compound-B. Ann Neurol 2004;55:306–319.
4. Fodero-Tavoletti MT, Smith DP, McLean CA, et al. *In vitro* characterization of Pittsburgh compound-B binding to Lewy bodies. J Neurosci 2007;27:10365–10371.
5. Maetzler W, Liepelt I, Reimold M, et al. Cortical PIB binding in Lewy body disease is associated with Alzheimer-like characteristics. Neurobiol Dis 2009;34:107–112.
6. Edison P, Rowe CC, Rinne JO, et al. Amyloid load in Parkinson's disease dementia and Lewy body dementia measured with [^{11}C]PIB positron emission tomography. J Neurol Neurosurg Psychiatry 2008;79:1331–1338.
7. Weintraub D, Dietz N, Duda JE, et al. Alzheimer's disease pattern of brain atrophy predicts cognitive decline in Parkinson's disease. Brain 2012;135:170–180.
8. McKeith IG, Dickson DW, Lowe J, et al.; the Consortium on DLB. Diagnosis and management of dementia with Lewy bodies: third report of the DLB Consortium. Neurology 2005;65:1863–1872.
9. Larsen JP, Dupont E, Tandberg E. Clinical diagnosis of Parkinson's disease. Proposal of diagnostic subgroups classified at different levels of confidence. Acta Neurol Scand 1994;89:242–251.
10. American Psychiatric Association. Diagnostic and Statistical Manual of Mental Disorders, 4th ed. Washington, DC: American Psychological Association; 2000.
11. McKhann G, Drachman D, Folstein M, Katzman R, Price D, Stadlan EM. Clinical diagnosis of Alzheimer's disease: report of the NINCDS-ADRDA Work Group under the auspices of Department of Health and Human Services Task Force on Alzheimer's Disease. Neurology 1984;34:939–944.
12. Folstein MF, Folstein SE, McHugh PR. "Mini-mental state". A practical method for grading the cognitive state of patients for the clinician. J Psychiatr Res 1975;12:189–198.
13. Dubois B, Slachevsky A, Litvan I, Pillon B. The FAB: a Frontal Assessment Battery at bedside. Neurology 2000;55:1621–1626.
14. Cummings JL, Mega M, Gray K, Rosenberg-Thompson S, Carusi DA, Gornbein J. The Neuropsychiatric Inventory: comprehensive assessment of psychopathology in dementia. Neurology 1994;44:2308–2314.
15. Fahn S, Elton R. Unified Parkinson's Disease Rating Scale. In: Fahn S, Marsden C, Calne D, Goldstein M, eds. Recent Developments in Parkinson's Disease. Florham Park, NJ: Macmillan Healthcare Information;1987:153e63.
16. Price JC, Klunk WE, Lopresti BJ, et al. Kinetic modeling of amyloid binding in humans using PET imaging and Pittsburgh Compound-B. J Cereb Blood Flow Metab 2005;25:1528–1547.
17. Lopresti BJ, Klunk WE, Mathis CA, et al. Simplified quantification of Pittsburgh Compound B amyloid imaging PET studies: a comparative analysis. J Nucl Med 2005;46:1959–1972.
18. Maldjian JA, Laurienti PJ, Kraft RA, Burdette JH. An automated method for neuroanatomic and cytoarchitectonic atlas-based interrogation of fMRI data sets. Neuroimage 2003;19:1233–1239.
19. Ashburner J, Friston KJ. Voxel-based morphometry—the methods. Neuroimage 2000;11:805–821.
20. Ashburner J, Friston KJ. Unified segmentation. Neuroimage 2005;26:839–851.
21. Beyer MK, Larsen JP, Aarsland D. Gray matter atrophy in Parkinson disease with dementia and dementia with Lewy bodies. Neurology 2007;69:747–754.
22. Burton EJ, McKeith IG, Burn DJ, Williams ED, O'Brien JT. Cerebral atrophy in Parkinson's disease with and without dementia: a comparison with Alzheimer's disease, dementia with Lewy bodies, and controls. Brain 2004;127:791–800.
23. Kempster PA, O'Sullivan SS, Holton JL, Revesz T, Lees AJ. Relationships between age and late progression of Parkinson's disease: a clinico-pathological study. Brain 2010;133:1755–1762.
24. Compta Y, Parkkinen L, O'Sullivan SS, et al. Lewy- and Alzheimer-type pathologies in Parkinson's disease dementia: which is more important?Brain 2011;134:1493–1505.
25. Foster ER, Campbell MC, Burack MA, et al. Amyloid imaging of Lewy body-associated disorders. Mov Disord 2010;25:2516–2523.
26. Rowe CC, Ng S, Ackermann U, et al. Imaging beta-amyloid burden in aging and dementia. Neurology 2007;68:1718–1725.
27. Chételat G, Villemagne VL, Bourgeat P, et al.; the Australian Imaging Biomarkers and Lifestyle Research Group. Relationship between atrophy and beta-amyloid deposition in Alzheimer disease. Ann Neurol 2010;67:317–324.
28. Ballard C, Ziabreva I, Perry R, et al. Differences in neuropathologic characteristics across the Lewy body dementia spectrum. Neurology 2006;67:1931–1934.
29. Mirra SS, Heyman A, McKeel D, et al. The Consortium to Establish a Registry for Alzheimer's Disease (CERAD). Part II. Standardization of the neuropathologic assessment of Alzheimer's disease. Neurology 1991;41:479–486.
30. Graff-Radford J, Boeve BF, Pedraza O, et al. Imaging and acetylcholinesterase inhibitor response in dementia with Lewy bodies. Brain 2012;135:2470–2477.

Cardiac Positron-Emission Tomography Images With an Amyloid-Specific Tracer in Familial Transthyretin-Related Systemic Amyloidosis

Katsutoshi Furukawa, MD, PhD; Shu-ichi Ikeda, MD, PhD; Nobuyuki Okamura, MD, PhD; Manabu Tashiro, MD, PhD; Naoki Tomita, MD, PhD; Shozo Furumoto, PhD; Ren Iwata, PhD; Kazuhiko Yanai, MD, PhD; Yukitsuka Kudo, PhD; Hiroyuki Arai, MD, PhD

We report the case of a 32-year-old man who had suffered from orthostatic syncope and body weight loss since he was 27 years old. As years passed by, he also showed muscle weakness and abnormal sensations in both legs, hyporeflexia in 4 limbs, and autonomic failure (impotence, urinary and fecal incontinence, and edema in lower limbs) suggesting the presence of peripheral somatic and autonomic polyneuropathy. His mother, mother's father, and mother's paternal aunt also had similar symptoms. Both the sensory nerve action potential and the sensory nerve conduction velocity of his right sural nerve were low (1.26 μV and 47.2 m/s, respectively), and the motor nerve conduction velocity of his right tibial nerve was 41.1 m/s (normal >45 m/s). A DNA test on the man disclosed a missense mutation in the transthyretin gene (Ser50Arg), which is relatively rare in familial transthyretin-related systemic amyloidosis.[1,2] Transthyretin-immunoreactive amyloid deposition was demonstrated in the biopsied gastroduodenal mucosa (Figure 1). Echocardiography showed a markedly thickened ventricular wall (thickness of interventricular septum 22.3 mm [normal <12 mm]) with normal wall motion (fractional shortening 37.6% [normal 28–42%]), indicating that he also had cardiac

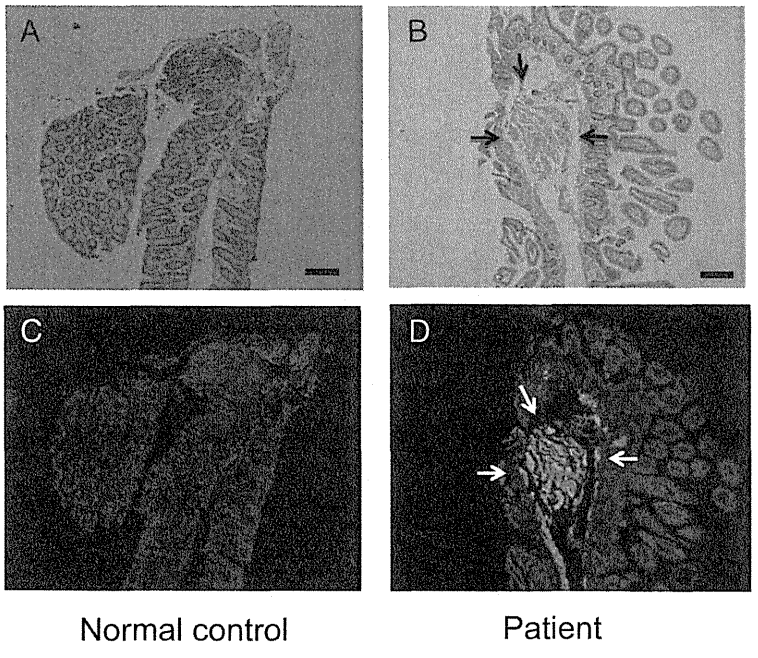

Figure 1. Detection of amyloid deposition in the intestines. Congo red (**A** and **B**) and BF-227 (**C** and **D**) clearly detect transthyretin in the submucosal space of the small intestine of the patient. Scale bars, 100 μm.

From the Department of Geriatrics and Gerontology, Division of Brain Sciences, Institute of Development, Aging and Cancer, Tohoku University (K.F., N.T., H.A.); Department of Medicine (Neurology & Rheumatology), Shinshu University School of Medicine (S.I.); Department of Pharmacology, Tohoku University Graduate School of Medicine (N.O., S.F., K.Y.); Division of Cyclotron Nuclear Medicine, Cyclotron and Radioisotope Center, Tohoku University (M.T.); Division of Radiopharmaceutical Chemistry, Cyclotron and Radioisotope Center, Tohoku University (R.I.); Department of NeuroImaging Research, Innovation New Biomedical Engineering Center, Tohoku University (Y.K.), Sendai, Japan.

Correspondence to Katsutoshi Furukawa, MD, PhD, Department of Geriatrics and Gerontology, Institute of Development, Aging and Cancer, Tohoku University, 4-1 Seiryo-machi Aobaku, Sendai 980-8575 Japan. E-mail kfurukawa-ns@umin.ac.jp

(*Circulation*. **2012;125:556-557.**)

Circulation **is available at http://circ.ahajournals.org** **DOI: 10.1161/CIRCULATIONAHA.111.045237**

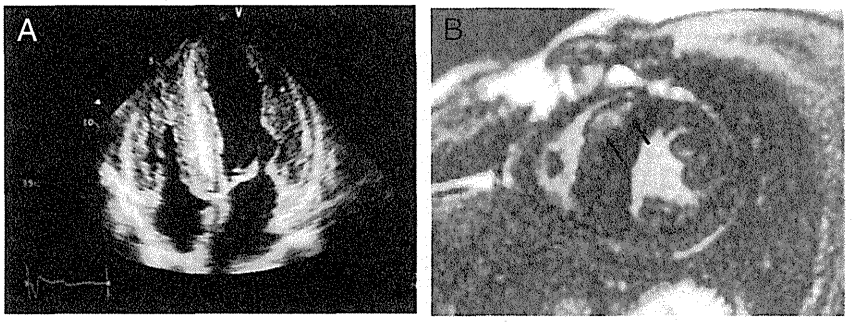

Figure 2. A, Echocardiographic finding. Four chamber views show symmetrical thickening of ventricular walls and septum with hyperrefractile myocardial echo (the so-called granular sparkling appearance). **B**, Contrast magnetic resonance imaging with gadolinium. Focal late gadolinium enhancement is visible (arrows).

amyloidosis (Figure 2A). Contrast magnetic resonance imaging[3] revealed focal late gadolinium enhancement in the thickened ventricular wall (Figure 2B). The patient had been treated with orthotopic live-donor liver transplantation when he was 31 years old to alleviate and prevent exacerbation of his neuronal and cardiac symptoms. His condition, including the neurological disability, gradually improved, and he started to work again 10 months after liver transplantation.

In order to visualize amyloid deposition in the myocardium, the patient underwent a cardiac positron-emission tomography study with [^{11}C]-BF-227 that sensitively and specifically binds to aggregated amyloid fibrils.[4] The positron-emission tomography images revealed significantly robust retention of [^{11}C]-BF-227 in the patient's heart compared with that of the normal control (Figure 3). Biopsy specimens from the patient's duodenum also showed higher signals of BF-227 compared with that of the normal control (Figure 1, C and D). The present result provides evidence that our amyloid-specific positron-emission tomography tracer, [^{11}C]-BF-227, can successfully detect amyloid deposition in the heart. Several molecules, such as ^{99m}Tc-aprotinin and ^{99m}Tc-labeled phosphate derivatives, have been investigated to visualize cardiac amyloidosis.[2] None of the previous tracers, however, could specifically bind to aggregated amyloid, which forms a β-pleated sheet structure. In any of the amyloidgenic disorders, such as transthyretin-related systemic amyloidosis and Alzheimer's disease, it is surmised that the monomer of the amyloid protein itself is not very toxic, whereas misfolded oligomers could cause damage to human organs.[1–4] It is therefore truly important to detect the accumulation of real amyloid fibrils for the early and accurate diagnosis of amyloidosis. To our knowledge, this is the first report showing the usefulness of a β-pleated sheet structure-specific positron-emission tomography in investing visceral organ amyloidosis.

Sources of Funding

This study was supported by the Program for the Promotion of Fundamental Studies in Health Science by the National Institute of Biomedical Innovation; the Special Coordination Funds for Promoting Science and Technology; the Industrial Technology Research Grant Program from the New Energy and Industrial Technology Development Organization of Japan; Health and Labor Sciences Research Grants for Translational Research from the Ministry of Health; and the Ministry of Education, Culture, Sports and Technology of Japan.

Acknowledgments

We appreciate technical assistance of Shoichi Watanuki, Yoichi Ishikawa, Motohisa Kato, and Emiko Fukuda.

Disclosures

None.

References

1. Ikeda S, Nakazato M, Ando Y, Sobue G. Familial transthyretin-type amyloid polyneuropathy in Japan: Clinical and genetic heterogeneity. *Neurology*. 2002;58:1001–1007.
2. Rapezzi C, Quarta CC, Riva L, Longhi S, Gallelli I, Lorenzini M, Ciliberti P, Biagini E, Salvi F, Branzi A. Transthyretin-related amyloidoses and the heart: a clinical overview. *Nat Rev Cardiol*. 2010;7:398–408.
3. Vogelsberg H, Mahrholdt H, Deluigi CC, Yilmaz A, Kispert Eva M, Greulich S, Klingel K, Kandolf R, Sechtem U. Cardiovascular magnetic resonance in clinically suspected cardiac amyloidosis. *J Am Coll Cardiol*. 2008;s51:1022–1030.
4. Furukawa K, Okamura N, Tashiro M, Waragai M, Furumoto S, Iwata R, Yanai K, Kudo Y, Arai H. Amyloid PET in mild cognitive impairment and Alzheimer's disease with BF-227: Comparison to FDG-PET. *J Neurol*. 2010;257:721–727.

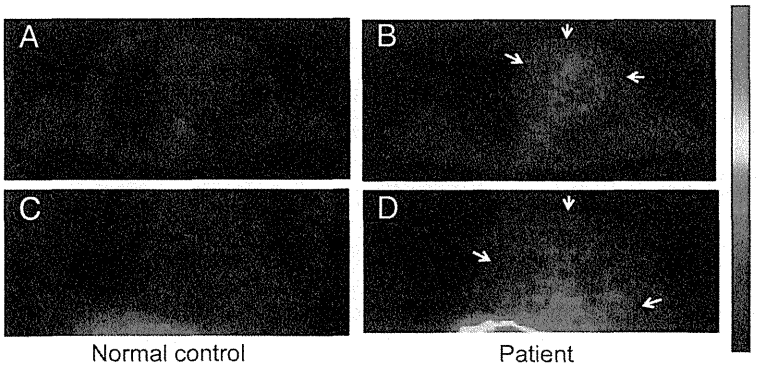

Figure 3. [^{11}C]-BF-227 positron emission tomgraphy succeeds in visualization of amyloid deposition in the heart. Axial and coronal images are **A** and **B** and **C** and **D**, respectively. Arrows indicate high signals of [^{11}C]-BF-227 in the heart of the patient (**B** and **D**).

MOLECULAR IMAGING AND BIOLOGY

Mol Imaging Biol (2013)
DOI: 10.1007/s11307-012-0608-5

World Molecular Imaging Society

RESEARCH ARTICLE

A ^{18}F-Labeled BF-227 Derivative as a Potential Radioligand for Imaging Dense Amyloid Plaques by Positron Emission Tomography

Shozo Furumoto,[1,2] Nobuyuki Okamura,[1] Katsutoshi Furukawa,[3] Manabu Tashiro,[4] Yoichi Ishikawa,[2] Kentaro Sugi,[1] Naoki Tomita,[3] Masaaki Waragai,[3] Ryuichi Harada,[1] Tetsuro Tago,[2] Ren Iwata,[2] Kazuhiko Yanai,[1] Hiroyuki Arai,[3] Yukitsuka Kudo[5]

[1]*Department of Pharmacology, Tohoku University School of Medicine, 2-1 Seiryo-machi, Aoba-ku, Sendai 980-8575, Japan*
[2]*Division of Radiopharmaceutical Chemistry, Cyclotron and Radioisotope Center, Tohoku University, Sendai, Japan*
[3]*Department of Geriatrics and Gerontology, Division of Brain Sciences, Institute of Development, Aging and Cancer, Tohoku University, Sendai, Japan*
[4]*Division of Cyclotron Nuclear Medicine, Cyclotron and Radioisotope Center, Tohoku University, Sendai, Japan*
[5]*Clinical Research, Innovation and Education Center, Tohoku University Hospital, Sendai, Japan*

Abstract

Purpose: The aims of this study were to evaluate the binding and pharmacokinetics of novel ^{18}F-labeled ethenyl-benzoxazole derivatives (i.e., [^{18}F] fluorinated amyloid imaging compound of Tohoku university ([^{18}F]FACT)) as amyloid positron emission tomography (PET) tracers and to assess [^{18}F]FACT efficacy in imaging of Alzheimer's disease (AD).

Procedures: Binding assay was conducted using synthetic amyloid-β (Aβ) fibrils, fluorescence microscopy, and autoradiogram in three postmortem AD brains. Pharmacokinetics of [^{18}F]FACT was assessed using 12 Crj:CD-1 (ICR) mice. *In vivo* binding ability with brain amyloid was investigated using amyloid precursor protein (APP) transgenic mouse. Clinical PET scanning using [^{18}F]FACT was performed in ten healthy controls and ten mild cognitive impairment and ten AD patients.

Results: [^{18}F]FACT showed high binding affinity for synthetic Aβ fibrils, preferential binding to dense cored plaques in brain sections, and excellent brain uptake and rapid clearance in mice. Injection in APP mice resulted in specific *in vivo* labeling of amyloid deposits in the brain. PET scans of AD patients showed significantly higher [^{18}F]FACT uptake in the neocortex compared to controls ($P<0.05$, Kruskal–Wallis test).

Conclusion: [^{18}F]FACT is a promising agent for imaging dense Aβ plaques in AD.

Key words: Alzheimer's disease, Amyloid, Early diagnosis, Positron emission tomography

Introduction

Alzheimer's disease (AD) is an age-dependent and irreversible neurodegenerative disorder leading to deterioration of memory and cognitive function. Although the exact mechanisms underlying pathogenesis of AD are not fully understood, formation of brain amyloid plaques through aggregation and deposition of amyloid-β protein (Aβ) is considered to be the initial pathogenic event that may precede the appearance of clinical AD symptoms by decades. Recently, new criteria for diagnosing AD were proposed by the National Institute on Aging—Alzheimer's Association workgroups [1]. The new diagnostic criteria include the use of biomarkers for amyloid deposition to aid

Correspondence to: Nobuyuki Okamura; *e-mail:* nookamura@med.tohoku.ac.jp

Published online: 30 January 2013

in diagnosis of AD. Thus, *in vivo* detection of amyloid depositions with positron emission tomography (PET) has received much attention as a potential technology for early or presymptomatic diagnosis of AD. For this purpose, a number of radiotracers for Aβ aggregates have been synthesized and evaluated as candidates for PET amyloid imaging agents, and some of these are undergoing clinical investigation [2–4].

Among them, *N*-methyl-[^{11}C]-2-(4′-methylaminophenyl)-6-hydroxybenzothiazole ([^{11}C]Pittsburgh compound B, [^{11}C]PiB) is currently the most widely used in clinical research [5]. Labeling of PET tracers with ^{18}F ($T_{1/2}$= 109.8 min) allows time for their delivery to numerous PET centers and contributes to spreading their use. Several ^{18}F-labeled amyloid PET tracers, including [^{18}F]flutemetamol, [^{18}F]florbetaben, [^{18}F]florbetapir, and [^{18}F]AZD4694, have been developed, and to date, [^{18}F]florbetapir has become commercially available [6–9]. An increasing number of PET studies in humans have clearly demonstrated that amyloid PET is a potentially useful technique to visualize and quantify the distribution of Aβ plaques of AD patients [5]. In addition, a proportion of elderly normal subjects present with [^{11}C]PiB retention in the neocortex [10–12], suggesting that amyloid PET is potentially useful for presymptomatic detection of Aβ pathology. Although neocortical PiB retention is considered as a high risk for future cognitive decline, not all PiB-positive normal individuals are destined to develop dementia. Some additional biomarkers are thus necessary for accurate prediction of future conversion to dementia. According to previous histopathological study, progression to dementia is associated with a shift from non-fibrillar to fibrillar amyloid deposits in the brain [13]. Thus, selective detection of dense fibrillar amyloid might be advantageous for predicting progression to dementia.

Previously, we had succeeded in developing a unique scaffold of a radioligand, [^{11}C]2-(2-[2-dimethylaminothiazol-5-yl]ethenyl)-6-(2-[fluoro]ethoxy)benzoxazole ([^{11}C]BF-227), as an amyloid imaging probe [3, 14]. Our previous study demonstrated that Aβ deposits in AD patients can be clearly detected by [^{11}C]BF-227 PET [15]. Neocortical [^{11}C]BF-227 retention was further observed in subjects with mild cognitive impairment (MCI) [16]. Using [^{11}C]BF-227 PET, we achieved a sensitivity of 100 % and a specificity of 71.4 % in distinguishing MCI converters to AD from MCI non-converters [17], suggesting the usefulness of this radiotracer for accurate prediction of future progression to dementia. To further take advantage of this imaging potential, especially in a large clinical study, we anticipated that a ^{18}F-labeled derivative of BF-227 would be valuable due to the longer half-life of ^{18}F compared with ^{11}C.

In this study, we performed a biological evaluation of a series of ^{18}F-labeled 2-ethenyl-benzoxazole derivatives (Fig. 1) to select a candidate for clinical application. The one selected, [^{18}F]Fluorinated Amyloid Imaging Compound of Tohoku University ([^{18}F]FACT), was further evaluated for its binding characteristics with Aβ fibrils and plaques and then for its clinical utility as a probe for imaging amyloid in AD.

Methods

Radiosynthesis of ^{18}F-Labeled 2-Ethenyl-Benzoxazole Derivatives

The chemical structures of the 2-ethenyl-benzoxazole derivatives are summarized in Fig. 1. The compounds and their precursors for ^{18}F-labeling were synthesized according to the method described previously [18]. ^{18}F-labeled compounds were prepared according to the following method. The aqueous $^{18}F^-$ contained in K_2CO_3 solution (1.27 to 3.28 GBq) and Kryptofix 2.2.2 were put into a brown vial, and then the water was azeotropically removed with acetonitrile by heating at 110 °C and He-gas flow. After drying, the activated [^{18}F]KF/Kryptofix 2.2.2. was reacted with a tosylate precursor in dimethyl sulfoxide (DMSO) at 110 °C for 10 min, followed by addition of water to quench. The product was extracted by solid-phase extraction with Sep-Pak ^{t}C18 cartridge (Waters) and then eluted with ethanol. The ^{18}F-labeled compound was separated from the eluent by semi-preparative reversed-phase high-performance liquid chromatography (RP-HPLC), isolated from the collected fraction by solid-phase extraction with Sep-Pak ^{t}C18

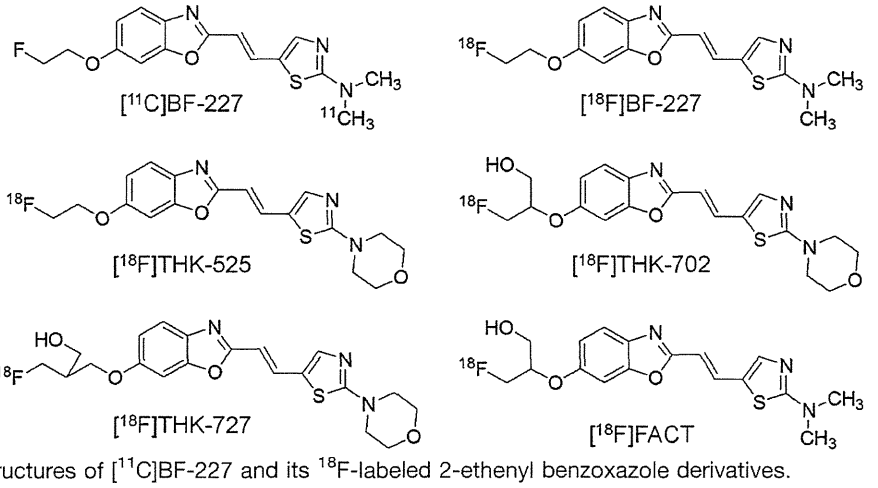

Fig. 1. Chemical structures of [^{11}C]BF-227 and its ^{18}F-labeled 2-ethenyl benzoxazole derivatives.

cartridge, and finally dissolved in DMSO or saline with polysorbate-80 (<0.1 %) for biological evaluation.

[^{11}C]BF-227 was synthesized from the precursor by *N*-methylation with [^{11}C]methyl triflate in DMSO and separated from the crude mixture by semi-preparative RP-HPLC, as described previously [15]. The purified [^{18}F]FACT and [^{11}C]BF-227 were solubilized in isotonic saline containing 1 % polysorbate-80 and 5 % ascorbic acid and then filter-sterilized with 0.22 μm Millipore filter for clinical use.

Fluorescent Staining

Postmortem brain tissue from a 69-year-old man with autopsy-confirmed AD was obtained from Fukushimura Hospital (Toyohashi, Japan). Experiments were performed under the regulations of the hospital ethics committee. Serial sections (6 μm) taken from paraffin-embedded blocks of the temporal cortex were prepared in xylene and ethanol. Before staining with test compounds, quenching of autofluorescence was performed. The quenched tissue section was immersed in 100 μM of test compounds containing 50 % ethanol for 10 min. The stained section was then dipped briefly into water before coverslipping with FluorSave Reagent (Calbiochem, La Jolla, CA, USA) and examination using an Eclipse E800 microscope (Nikon, Tokyo, Japan) equipped with a V-2A filter set (excitation 380 to 420 nm, dichroic mirror 430 nm, long pass filter 450 nm). An adjacent section was immunostained using 4G8 (Signet, Dedham, MA, USA), a monoclonal antibody against Aβ. After pretreatment with 90 % formic acid for 5 min, sections were immersed in blocking solution for 30 min and then incubated for 60 min at 37 °C with 4G8 at a dilution of 1:100. After incubation, sections were processed with biotinylated anti-mouse IgG (Wako) for 60 min, followed by Texas Red-conjugated streptavidin (Vector Laboratories, Burlingame, CA, USA).

In Vitro Autoradiography

A temporal brain section from a 76-year-old female AD patient was incubated with 1.85 MBq/ml of [^{18}F]FACT at room temperature for 20 min and then washed briefly with water and 70 % ethanol. After drying, the labeled section was exposed to a BAS-III imaging plate (Fuji Film, Tokyo, Japan) for 120 min. Autoradiograms were obtained using a BAS-5000 phosphor imaging instrument (Fuji Film, Tokyo, Japan). Neighboring sections were immunostained using 4G8 anti-Aβ monoclonal antibody. After incubation with 4G8, sections were processed by the avidin–biotin method using a Pathostain ABC-POD(M) Kit (Wako, Osaka, Japan) and diaminobenzidine tetrahydrochloride.

In Vitro Binding Study

Amyloid β_{1-40} (Peptide Institute, Inc., Japan) was dissolved in 50 mM potassium phosphate buffer (pH 7.4) to a final concentration of 20 μM. To prepare amyloid fibrils, the solution was incubated at 37 °C for 4 days at 85 rpm and then sonicated to obtain a uniform suspension. The fibril solution was diluted to 2 μM with phosphate-buffered saline (PBS) containing 0.1 % bovine serum albumin (BSA). For saturation binding assay, 100 μl of the fibril solution was mixed with [^{18}F]FACT solution (0.2 to 800 nM, PBS containing 0.1 % BSA and 2 % DMSO, 100 μl) in a 96-well plate. Non-specific binding was defined in the presence of 2 μM FACT in the final solution. The mixture was incubated for 40 min at room temperature and then was passed through the glass filter plate under vacuum with MultiScreen HTS Vacuum Manifold (Millipore Corp., USA), followed by washing with PBS containing 0.1 % BSA twice. Radioactivity of the filter was counted with an automatic gamma counter. The binding data were analyzed with curve-fitting software that calculates the K_d and B_{max} using non-linear regression (GraphPad Prism Version 5.0, GraphPad Software, San Diego, CA, USA).

Biodistribution Study in Normal Mice

The experimental protocols were reviewed by the Committee on the Ethics of Animal Experiments at Tohoku University School of Medicine and performed in accordance with the Guidelines for Animal Experiments issued by the Tohoku University School of Medicine. Male Crj:CD-1 (ICR) mice (6 weeks old, 25 to 30 g, n=12) were injected in a lateral tail vein with ^{18}F-labeled test compounds (370 to 740 kBq) contained in isotonic saline (0.2 ml). The mice were sacrificed by cervical dislocation following heart puncture to obtain blood samples at 2, 30, and 60 min postinjection (n=4 at each time point). Tissues of interest were excised and weighed, and the radioactivity was counted in an automatic gamma-counter. Radioactivity uptake data are expressed as percent of injected dose per gram of tissue (%ID/g).

Autoradiography of Aβ Deposits in Living Transgenic Mice

An amyloid precursor protein (APP) transgenic (Tg) mouse (female, 31 months old) and a wild-type littermate (female, 31 months old) were injected with [^{18}F]FACT (37 MBq) *via* tail vein. The mice were sacrificed by cervical dislocation at 2 h postinjection, and the brains were rapidly excised and frozen in liquid nitrogen. Frozen sections of 20 μm thick were prepared from the brains for *ex vivo* autoradiography. Autoradiograms were obtained in the same manner described above. The sections used for autoradiography were then subjected to fluorescent staining with thioflavin-S according to the previously described method [19].

Clinical PET Study Using [^{18}F]FACT

Ten patients with amnestic MCI, ten patients with AD, and ten normal age-matched controls participated in the clinical PET study using [^{18}F]FACT. Please refer to Table 1 for characteristics of participants. [^{11}C]BF-227 PET scan was additionally performed in two patients with AD (70-year-old woman (MMSE score 17) and 79-year-old man (MMSE score 20)) and 1 normal control subject (60-year-old man (MMSE score 30)). The average time interval between [^{18}F]FACT and [^{11}C]BF-227 PET scans was 12±6 months. Diagnosis of probable AD was based on criteria from the National Institute of Neurological and Communicative Disorders and Stroke and the Alzheimer's Disease Related Disorders Association [20]. The diagnosis of amnestic MCI was made according to published criteria described previously [21]. The control subjects were

Table 1. Subject and patient demographics in [^{18}F]FACT PET comparisons

	NC	MCI	AD
N	10	10	10
Gender (F/M)	4/6	7/3	7/3
Age (years)	69.8±8.8 (60–89)	74.2±8.8 (57–89)	74.5±4.6 (66–81)
MMSE score	29.9±0.3 (29–30)	26.4±1.1 (24–28)	19.8±3.0 (15–24)

recruited from volunteers who were taking no centrally acting medications, had no cognitive impairment, and had no cerebrovascular lesions, including asymptomatic cerebral infarction on T2-weighted studies, identified *via* MRI. All volunteers were screened using a questionnaire and medical history, and those with medical conditions potentially affecting the central nervous system were excluded. The Committee on Clinical Investigation at Tohoku University School of Medicine and the Advisory Committee on Radioactive Substances at Tohoku University approved the study protocol. After complete description of the study to the patients and subjects, written informed consent was obtained.

Image Acquisition Protocols

[^{18}F]FACT-PET and [^{11}C]BF-227-PET study was performed using a SET-2400W PET scanner (Shimadzu, Kyoto, Japan). After intravenous injection of 111–185 MBq of [^{18}F]FACT or 211–366 MBq of [^{11}C]BF-227, dynamic PET images were obtained for 60 min (23 sequential scans; 5 scans×30 s, 5 scans×60 s, 5 scans×150 s, and 8 scans×300 s) with the subject's eyes closed. SUV summation images at 0–10, 10–20, 20–30, 30–40, 40–50, and 50–60 min postinjection were created for the analysis of tracer uptake. T1-weighted MR images were obtained using a SIGNA 1.5 T machine (General Electric, Milwaukee, WI, USA).

Image Analysis

Firstly, standardized uptake value (SUV) images of [^{18}F]FACT and [^{11}C]BF-227 were obtained by normalizing tissue radioactivity concentration by injected dose and body weight. Subsequently, individual MR images were anatomically coregistered into individual PET images using Statistical Parametric Mapping software (SPM5: Welcome Department, UK). Regions of interest (ROIs) were placed on individual axial MR images in the cerebellar hemisphere, frontal cortex [Brodmann's areas (BA) 8, 9, 10, 44, 45, 46, and 47], lateral temporal cortex (BA 21, 22, 37, and 38), parietal cortex (BA 39 and 40), occipital cortex (BA 17), anterior cingulate cortex, posterior cingulate cortex, medial temporal cortex (BA 27, 28, 34, and 35), striatum, pons, and subcortical white matter, as described previously [15]. The ROI information was then copied onto dynamic PET SUV images, and regional SUVs were sampled using PMOD software (PMOD Technologies, Ltd., Zurich, Switzerland). The ratio of regional SUV to cerebellar SUV (SUVR) was calculated as an index of tracer retention. Averaged SUVR in the frontal, temporal, parietal, and posterior cingulate cortices was considered representative of tracer retention in the neocortex (neocortical SUVR). The inter-rater reliability for the ROI measurement was tested between two raters (N.O. and K.S.) in seven subjects and patients. The intra-class correlation coefficient was 0.95.

Statistical Analysis

For statistical comparison in the three groups, we applied the Kruskal–Wallis test followed by Dunn's multiple comparison test. Differences of time activity curves (TACs) in [^{18}F]FACT PET were also evaluated by repeated measures ANOVA followed by the Bonferroni–Dunn post hoc test. For statistical comparisons of PET measurements in control and AD groups, we used the Mann–Whitney *U* test. Effect size coefficients (Cohen's *d*) were also calculated for the evaluation of group differences in PET measurements. Statistical significance for each analysis was defined as $P<0.05$. Correlations between [^{18}F]FACT and [^{11}C]BF-227 SUVR in the frontal, temporal, parietal, and occipital cortices of three subjects (two AD and one normal control) were determined using Pearson's correlations. A linear model was applied to the data to obtain a correlation coefficient and *p* value. These analyses were performed using GraphPad Prism5 software (GraphPad, San Diego, CA, USA).

Results

Radiosynthesis

^{18}F-labeled 2-ethenyl-benzoxazole derivatives (Fig. 1) were obtained in yields of 32 % on average (21 to 44 %, decay-corrected) with radiochemical purity greater than 99 % after HPLC purification. The specific activities ranged 70 to 180 GBq/μmol, corrected at the end of synthesis.

In Vitro Binding to Aβ Plaques in AD Brain Sections

Binding ability of 2-ethenyl-benzoxazole derivatives to Aβ plaques was examined using AD brain sections from a 69-year-old man with autopsy-confirmed AD. As shown in Fig. 2a, c, dense cored plaques (arrowheads) were clearly stained with FACT. In particular, Aβ plaque cores were brightly stained with this compound. The fluorescent staining pattern of FACT correlated well with Aβ immunostaining (Fig. 2b) and thioflavin-S staining (Fig. 2d) in adjacent sections. Other compounds produced similar results in the histopathological staining of AD brain sections from a 69-year-old man with autopsy-confirmed AD.

In vitro autoradiography at tracer dose indicated [^{18}F]FACT binding to dense Aβ deposits (arrowheads) in AD temporal brain sections from a 76-year-old female AD patient (Fig. 2e–h). Tracer signals were additionally detected

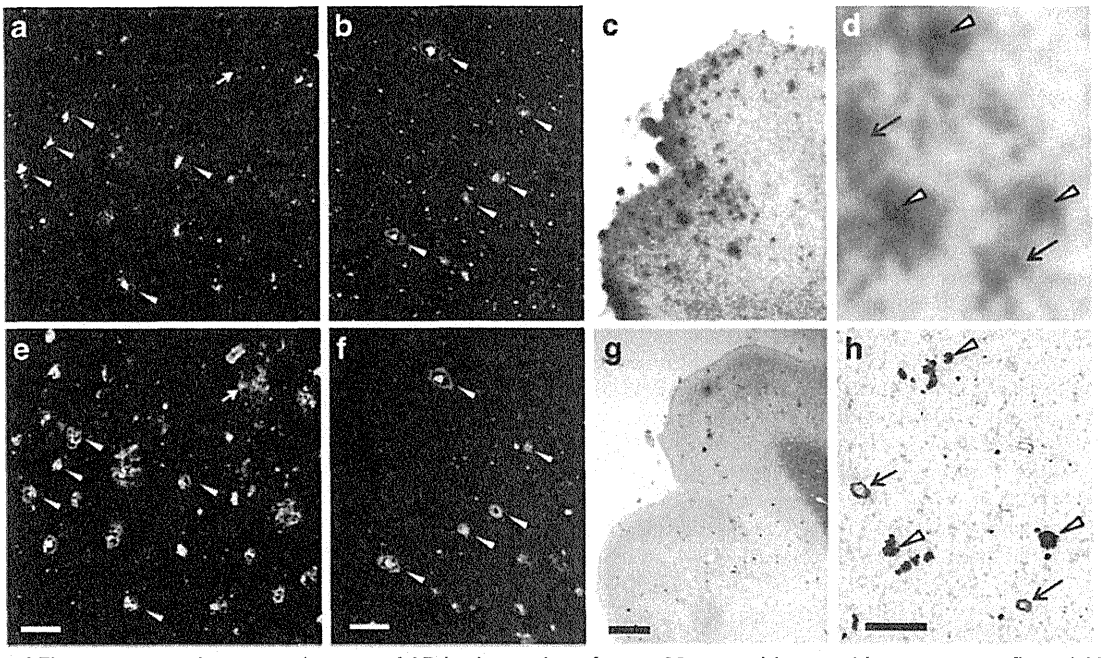

Fig. 2. **a–d** Fluorescence microscopy images of AD brain sections from a 69-year-old man with autopsy-confirmed AD stained with FACT (**a**, **c**), anti-Aβ (4 G8) antibody (**b**), and thioflavin-S (**d**). *Arrowheads* delineate dense cored plaques, respectively. **e–h** Autoradiogram of AD brain section from a 76-year-old female AD patient with [^{18}F]FACT (**e**, **g**) and images of the adjacent section immunostained with anti-Aβ (4 G8) antibody (**f**, **h**). *Arrows* and *arrowheads* delineate congophilic amyloid angiopathy and dense cored plaques, respectively. *Bars* 100 μm (**a–d**), 2 mm (**e–f**), 200 μm (**g–h**).

in congophilic amyloid angiopathy (arrows). These results indicated that FACT and its derivatives had an ability to detect pathological dense Aβ deposits in AD brain tissue.

Binding Affinity to Synthetic Aβ Fibrils

Binding properties of [^{18}F]FACT with Aβ fibrils were investigated by *in vitro* binding assay. Scatchard analysis of FACT binding to Aβ fibrils showed two classes of binding sites: a high-affinity site (K_d=9.4 nM; B_{max}= 0.16 pmol/nmol of Aβ) and a low-affinity site (K_d= 263 nM; B_{max}=1.52 pmol/nmol of Aβ).

Biodistribution Study in Normal Mice

Two important properties of an amyloid imaging probe are rapid brain uptake and rapid clearance from the normal brain without non-specific binding. These properties of the ^{18}F-labeled 2-ethenyl-benzoxazole derivatives were evaluated by biodistribution studies in 12 normal mice (n=4 at each time point). The radioactivity uptake in the blood, brain, liver, kidney, and bone is summarized in Table 2. Regarding brain uptake, all of the ^{18}F-labeled derivatives showed rapid and sufficient brain uptake (4 to 6 %ID/g at 2 min) and smooth washout after that. However, the brain uptake at 60 min varied from 0.28 to 1.68 %ID/g, suggesting a different clearance property in normal brain. Among the derivatives, [^{18}F]FACT indicated the highest ratio of brain uptakes at 2 min to that at 60 min (4.64/0.28=16.6). Additionally, mice injected with [^{18}F]FACT exhibited no increase of the radioactivity uptake in bone with time, unlike with [^{18}F]BF-227, suggesting that [^{18}F] FACT has good stability in regard to metabolic defluorination *in vivo*. Thus, we selected [^{18}F]FACT as the candidate for the clinical comparisons.

Autoradiography of Aβ Deposits in Living Transgenic Mouse

In vivo binding ability of [^{18}F]FACT with amyloid plaques was evaluated in the APP-Tg mouse. Autoradiographic images of the APP-Tg mouse brain post-intravenous injection of [^{18}F]FACT displayed high uptake of the labeling compound in the cortex and hippocampus (Fig. 3a). In contrast, no notable binding was observed in the brain of wild-type mouse (Fig. 3b). These [^{18}F]FACT binding results in APP-Tg mouse brain corresponded closely with those of *in vitro* thioflavin-S staining in the same brain sections (Fig. 3c, d). These results warranted further clinical investigation of [^{18}F]FACT PET in AD patients.

Clinical PET Study Using [^{18}F]FACT

Demographic data for the participants are summarized in Table 1. No statistical difference in age was observed among the three groups. MCI and AD patients had significantly lower mean MMSE scores than normal controls (P<0.05,

Table 2. Biodistribution of ^{18}F-labeled compounds in mice

Tracers	Time (min)	Radioactivity uptakes (%ID/g)				
		Blood	Brain	Liver	Kidney	Bone
[^{18}F]BF-227	2	2.93±0.08	6.05±0.45	7.97±1.59	9.63±0.89	1.59±0.27
	30	2.14±0.17	1.91±0.05	5.75±0.42	3.04±0.15	4.38±1.24
	60	2.09±0.15	1.67±0.14	5.48±0.23	2.42±0.20	7.04±0.75
[^{18}F]THK-525	2	2.82±0.38	4.73±1.32	5.93±1.40	7.72±2.44	1.77±0.87
	30	2.20±0.24	2.05±0.16	3.55±0.60	2.32±0.18	6.74±2.20
	60	1.91±0.29	1.68±0.15	2.47±0.23	1.48±0.14	9.65±0.89
[^{18}F]THK-702	2	3.34±0.13	4.15±0.28	7.53±0.50	13.6±0.88	1.95±0.34
	30	1.06±0.19	0.53±0.03	4.55±0.39	1.58±0.64	0.92±0.11
	60	0.67±0.08	0.35±0.04	3.65±0.72	0.65±0.09	1.16±0.70
[^{18}F]THK-727	2	2.94±0.33	4.06±0.26	9.89±4.16	11.4±1.35	2.08±0.39
	30	1.52±0.10	1.04±0.08	6.68±1.22	2.47±0.36	6.61±0.79
	60	0.66±0.10	0.69±0.02	4.04±1.87	0.98±0.14	9.33±1.34
[^{18}F]FACT	2	3.65±0.66	4.64±0.55	9.38±0.43	10.2±1.05	1.84±0.18
	30	1.19±0.49	0.53±0.11	11.3±1.32	4.17±0.44	0.88±0.07
	60	0.64±0.13	0.28±0.04	14.1±0.55	3.25±0.27	1.38±0.46

Data are expressed as mean±SD (n=4 at each time point)

Kruskal–Wallis test). AD patients additionally had significantly lower mean MMSE scores than those with MCI ($P<$ 0.05, Kruskal–Wallis test). No toxic events were observed in the current clinical trial. The SUV-TACs from [^{18}F]FACT-PET in AD patients and normal control subjects are shown in Fig. 4. Both groups showed rapid entry of [^{18}F]FACT into the neocortex and cerebellum. In the AD patients, the temporal cortex, known to contain high concentrations of fibrillar amyloid plaques in AD, showed retention of [^{18}F] FACT during the later time points compared with the cerebellum (Fig. 4a). In contrast, TACs in the temporal cortex and the cerebellum were nearly identical in normal subjects (Fig. 4b). The subcortical white matter regions showed relatively lower entry and slower clearance than gray matter areas, but no difference in TACs between AD patients and normal controls.

SUVR in the lateral temporal cortex of AD patients was significantly higher over 10 min postinjection of [^{18}F]FACT than those of normal controls ($p<0.05$, Mann–Whitney U test) and reached maximum value at 30 to 40 min postinjection (Fig. 4c). Effect size between AD and normal controls showed the highest value at 30 to 40 min postinjection of [^{18}F]FACT (Table 3). The ratio of SUVR in AD to SUVR in normal controls became constant after

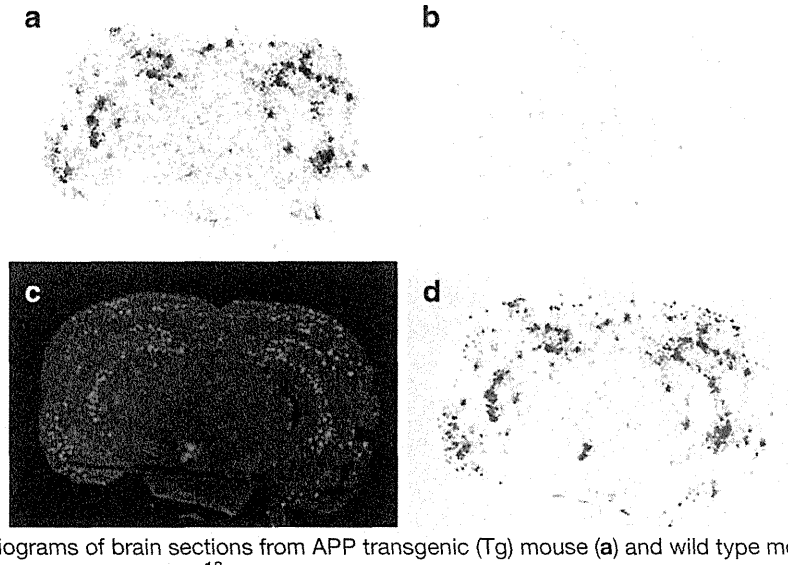

Fig. 3. *Ex vivo* autoradiograms of brain sections from APP transgenic (Tg) mouse (**a**) and wild type mouse (**b**). The brains were excised at 2 h after intravenous injection of [^{18}F]FACT. Aβ plaques in APP-Tg mouse brain were clearly stained with thioflavin-S (**c**). A merged image of **a** and **c** is shown in **d**.

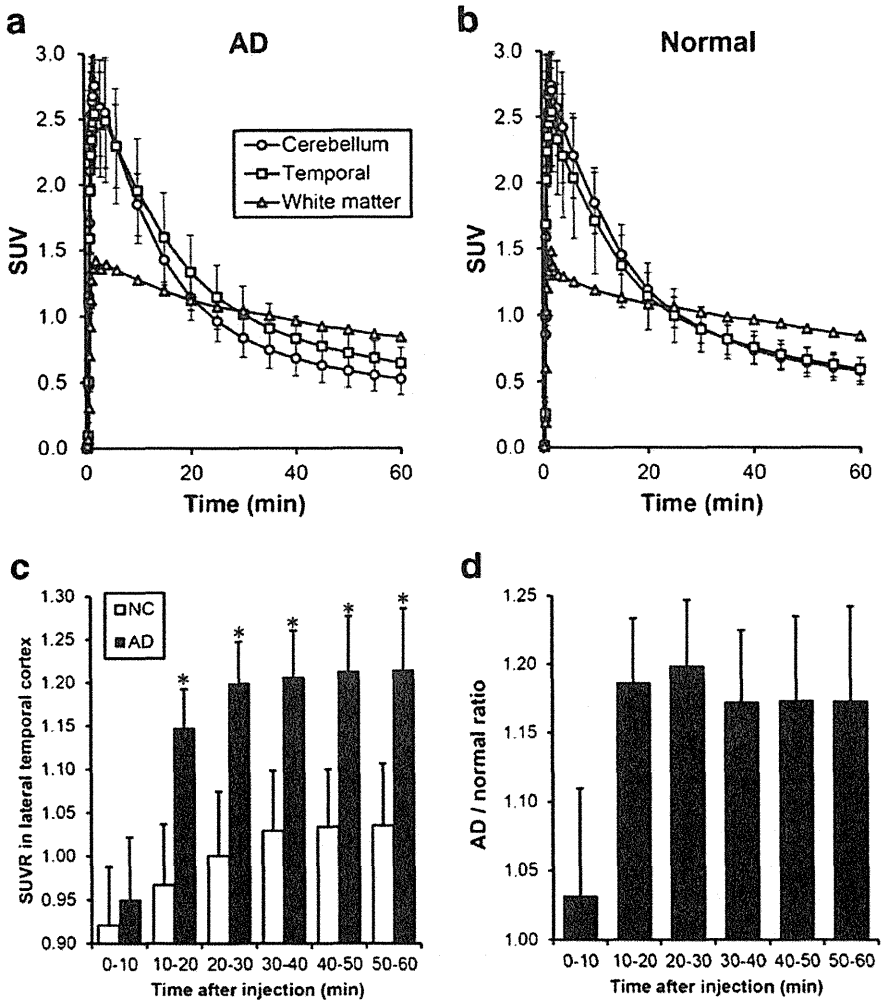

Fig. 4. Time activity data for [^{18}F]FACT PET in humans. Time activity curves of [^{18}F]FACT in ten AD patients (**a**) and ten normal controls (**b**) are shown. Each point represents the mean±standard deviations of data. Time course of [^{18}F]FACT SUVR in the lateral temporal cortex (**c**) and AD *vs* normal ratio of SUVR in the lateral temporal cortex (**d**) are also shown. *P<0.05 by the Mann–Whitney U test.

30 min (Fig. 4d). Based on these results, we selected summed dynamic images from 30 to 40 min for the ROI analysis of PET data.

SUVR images of [^{18}F]FACT for a normal control subject (a 60-year-old man, MMSE score 30) and an AD patient (70-year-old woman, MMSE score 17) are shown in Fig. 5a. Cortical retention of [^{18}F]FACT at 30 to 40 min postinjection was evident in the AD patient, as contrasted with the images of the normal control subject. This pattern of distribution was consistent with the distribution of [^{11}C]BF-227 at 30 to 40 min postinjection in the same subject and patient pair (Fig. 5a). The SUV-TACs from [^{18}F]FACT-PET were compared with those from [^{11}C]BF227-PET in the same AD patient (70-year-old woman, MMSE score 17). As shown in Fig. 5b, [^{18}F]FACT showed faster washout from both temporal cortex and cerebellum than [^{11}C]BF-227. The regional SUVR of [^{18}F]FACT at 30 to 40 min postinjection was compared with that of [^{11}C]BF-227 at the same time frame. SUVR values in the frontal, temporal, parietal, and occipital cortices of three subjects (two AD and one normal control) were used for this analysis. As shown in Fig. 5c, regional SUVR of [^{18}F]FACT were significantly correlated with that of [^{11}C]BF-227 (Pearson's r= 0.931, P<0.001) in these three subjects.

In the quantitative comparison of regional SUVR 30 to 40 min post-administration, the values for the frontal, lateral

Table 3. Time course of lateral temporal [^{18}F]FACT SUVR and effect size measures in ten normal controls and ten AD patients

Time (min)	Normal control	AD	Cohen's d
30–40	1.07±0.06	1.22±0.05*	2.67
40–50	1.08±0.06	1.23±0.06*	2.37
50–60	1.09±0.06	1.23±0.06*	2.34

*P<0.05 by the Mann–Whitney U test

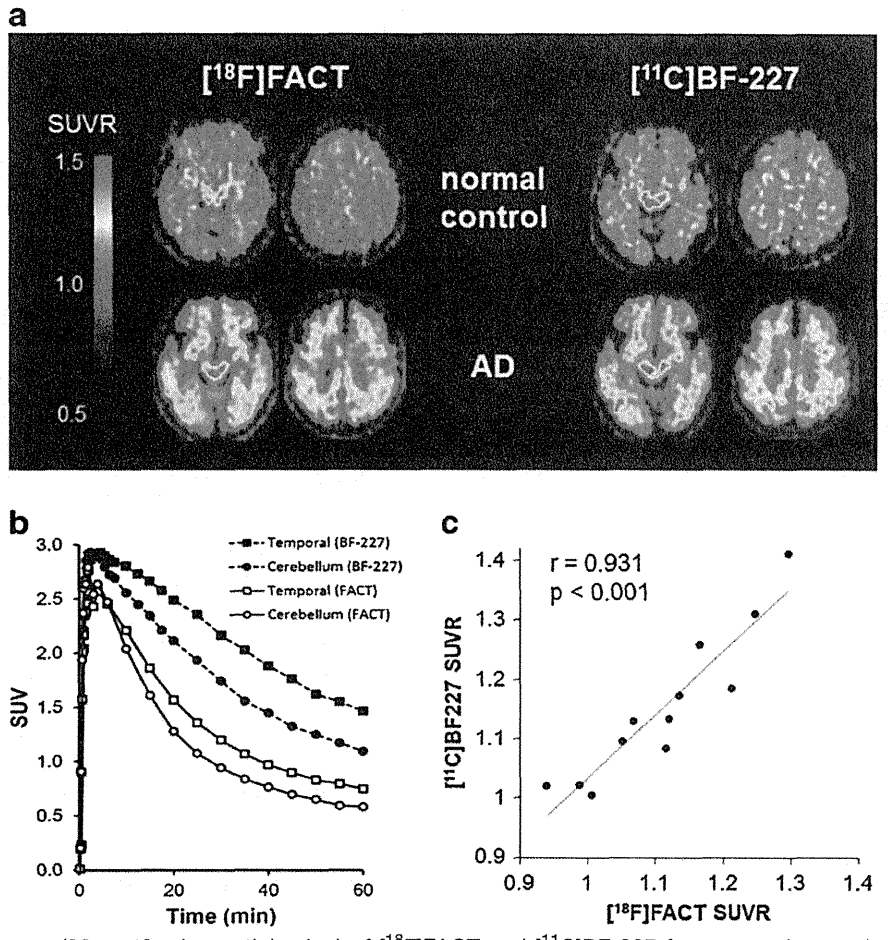

Fig. 5. **a** SUVR images (30 to 40 min postinjection) of [^{18}F]FACT and [^{11}C]BF-227 for a normal control subject (60-year-old man, MMSE score 30) and an AD patient (70-year-old woman, MMSE score 17). **b** Time activity curves of [^{18}F]FACT and [^{11}C]BF-227 in an AD patient (70-year-old woman, MMSE score 17). **c** Significant correlation between regional SUVR of [^{18}F]FACT and [^{11}C]BF-227 in two AD (70-year-old woman (MMSE score 17) and 79-year-old man (MMSE score 20)) and one normal control (60-year-old man, MMSE score 30) subjects (Pearson's r=0.931, P<0.001).

temporal, parietal, occipital, and anterior and posterior cingulate cortices were significantly greater in AD patients than in the normal controls (Table 4). In addition, the SUVRs for the lateral temporal, parietal, occipital, and anterior and posterior cingulate cortices were significantly greater in AD patients than in those with MCI. As shown in Fig. 6, averaged neocortical SUVR was also significantly greater in AD patients than in normal control subjects and MCI (P<0.05, Kruskal–Wallis test). MCI patients additionally showed significantly greater SUVR in the lateral temporal and frontal cortices than normal subjects, but not significant in other brain regions (P<0.05, Kruskal–Wallis

Table 4. Regional SUVR (30 to 40 min postinjection) and effect size measures of [^{18}F]FACT in ten normal controls and ten MCI and ten AD patients

	Normal control	MCI	AD	Cohen's d NC *vs.* AD
Frontal	1.00±0.10	1.09±0.04*	1.15±0.06*	1.82
Lateral temporal	1.05±0.08	1.13±0.06*	1.21±0.05*,**	2.40
Parietal	1.07±0.07	1.13±0.07	1.21±0.08*,**	1.86
Occipital	1.09±0.08	1.07±0.06	1.17±0.05*,**	1.20
Anterior cingulate	1.08±0.07	1.12±0.08	1.21±0.08*,**	1.73
Posterior cingulate	1.15±0.07	1.17±0.06	1.30±0.07*,**	2.14
Medial temporal	1.10±0.05	1.13±0.04	1.15±0.09	0.69
Striatum	1.31±0.11	1.30±0.06	1.35±0.12	0.35
Pons	1.55±0.15	1.57±0.10	1.54±0.09	0.08
White matter	1.50±0.21	1.47±0.11	1.52±0.13	0.12
Neocortex	1.04±0.07	1.12±0.05	1.19±0.05*,**	2.47

*P<0.05 (vs normal control group) and **P<0.05 (vs MCI group) by the Kruskal–Wallis test followed by Dunn's multiple comparison test

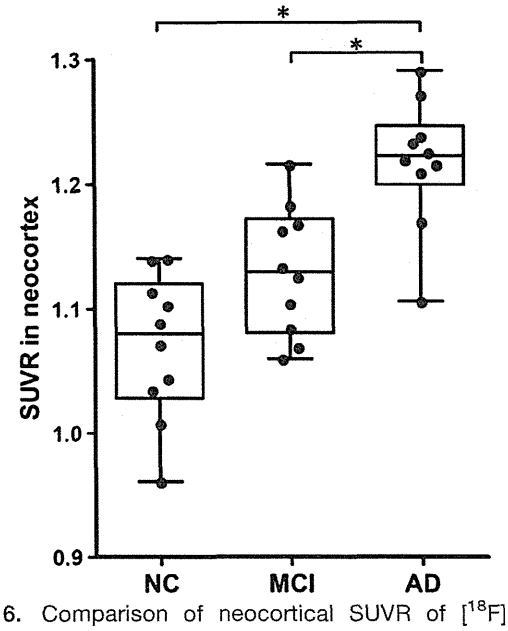

Fig. 6. Comparison of neocortical SUVR of [^{18}F]FACT among ten aged normal controls (NC) and ten mild cognitive impairment (MCI) and ten AD patients. The neocortical SUVRs are represented in a *box* and *whisker plot*. *P<0.05 by the Kruskal–Wallis test followed by Dunn's multiple comparison test.

test). The SUVR in the medial temporal cortex and striatum showed the tendency to be greater in AD patients, but this was not significant. The SUVR in the pons and white matter was nearly identical in AD, MCI, and normal subjects. Effect size value between AD and aged normal subjects was the highest in the lateral temporal cortex (2.40), followed by the posterior cingulate (2.14), parietal (1.86), frontal (1.82), and anterior cingulate (1.73) and occipital (1.20) cortices (Table 4).

Discussion

The current study demonstrated that [^{18}F]FACT PET can be used to detect AD pathology in AD patients and to confirm its absence in cognitively unimpaired elderly people. We previously reported the ability of [^{11}C]BF-227-PET to detect Aβ deposits in the brains of AD patients [15]. The current study has further demonstrated the binding preference of [^{18}F]FACT to dense Aβ plaques in the brains of AD patients. A similar pattern of tracer distribution was observed between [^{18}F]FACT and [^{11}C]BF-227 in AD patients, indicating that [^{18}F]FACT-PET could be substituted for [^{11}C]BF-227-PET for noninvasive detection of dense Aβ deposits in the brain of AD patients. The correlation of [^{18}F]FACT uptake *in vivo* and brain pathology at autopsy should be examined in the future. Our previous studies demonstrated the unique ability of [^{11}C]BF-227 to detect certain forms of prion and α-synuclein protein deposits [22, 23]. Further study will be required to validate the practical usefulness of [^{18}F]FACT-PET for noninvasive detection of these protein deposits.

When a neocortical [^{18}F]FACT SUVR of 1.145 (1.5 SD above control mean) was used as a cutoff, [^{18}F]FACT-PET scan achieved a sensitivity of 90 % (nine of ten) and a specificity of 100 % (ten of ten) in the discrimination between AD patients and normal subjects. In one exception, a 76-year-old female AD patient, MMSE score 24, showed no remarkable retention of [^{18}F]FACT in the neocortex. This is not surprising because approximately 10 to 20 % of patients diagnosed as probable AD reportedly fail to meet pathological criteria for AD at autopsy.

The amnestic subtype of MCI has a high risk of progression to dementia, and it may constitute a prodromal stage of AD [24]. Previous amyloid-PET studies demonstrated a substantial amount of neocortical tracer retention in 50 to 60 % of the MCI population, which is comparable to the level in AD patients [10, 17]. In our study, about half of the MCI patients had elevated neocortical [^{18}F]FACT retention, which was an intermediate level between the aged normal subjects and the AD patients. This finding is in accord with the previous neuropathological observation that the density of neuritic plaque increased as a function of increasing dementia severity [25]. The parent tracer [^{11}C]BF-227 showed neocortical retention to be a reliable indicator of disease progression in MCI subjects in our previous study [17, 19]. Therefore, PET imaging with [^{18}F]FACT is also expected to have a similar prognostic utility.

The amount of elevation of neocortical [^{18}F]FACT uptake in AD patients was approximately 14 to 15 %, far less than PiB and other ^{18}F-labeled amyloid-PET tracers. This is probably due to the relatively low binding affinity and B_{max} of this tracer with amyloid fibrils in comparison to that of PiB (K_d=1.02 nM, B_{max}=0.61) [26, 27]. There is considerable amount of tracer retention in the white matter, which reflects non-specific binding of the compound to myelin sheath. Because of modest specific binding of [^{18}F]FACT in the gray matter of AD patients, spillover from the white matter could reduce the sensitivity for detecting amyloid positive subjects. Use of early phase (30 to 40 min postinjection) images can compensate for this because the relatively stronger signals in the gray matter persist in this time interval. Partial volume correction may also be able to improve the discriminatory power of [^{18}F]FACT-PET by eliminating nonspecific signals in the white matter. Another method to improve the sensitivity for detecting specific signals in the brain is to create a statistical map by comparison with a normal control database [19].

One of advantages of [^{18}F]FACT over BF-227 is its rapid kinetic profile. [^{18}F]FACT showed faster washout from normal brain tissue than BF-227 (Fig. 5) probably because of the lower lipophilicity of FACT (LogP=1.99±0.02) as compared to BF-227 (LogP=2.29±0.02). The neocortical SUVR of [^{18}F]FACT reached a peak at 30 min post-administration. This characteristic would also contribute to reduced procedure and waiting times for PET scans.

Conclusion

We successfully developed a novel ^{18}F-labeled ethenylbenzoxazole derivative, [^{18}F]FACT, as a PET tracer for amyloid deposits. This tracer preferentially bound to dense Aβ plaques in AD brain sections, visualized cortical amyloid deposits in APP Tg mice, and demonstrated fast kinetics and significant retention of [^{18}F]FACT in sites with predilection for the deposition of dense amyloid plaques in AD patients during clinical PET imaging. [^{18}F]FACT PET distinctly distinguished AD patients from normal individuals. These findings suggest that [^{18}F]FACT may be usable for *in vivo* detection of dense Aβ plaques in AD brains.

Acknowledgments. This study was financially supported by the Special Coordination Funds for Promoting Science and Technology, the Health and Labour Sciences Research Grants for Translational research from Ministry of Health, Labour and Welfare, the Program for Promotion of Fundamental Studies in Health Science of the National Institute of Biomedical Innovation, and the Grant-in-Aid for Scientific Research (C) (20591432) from the Ministry of Education, Culture, Sports, Science and Technology of Japan. The authors appreciate the technical assistance of Dr. Shoichi Watanuki in the clinical PET studies.

Conflict of Interest. The authors declare they have no conflicts of interest.

References

1. McKhann GM, Knopman DS, Chertkow H et al (2011) The diagnosis of dementia due to Alzheimer's disease: recommendations from the National Institute on Aging—Alzheimer's Association workgroups on diagnostic guidelines for Alzheimer's disease. Alzheimers Dement 7:263–269
2. Kadir A, Nordberg A (2010) Target-specific PET probes for neurodegenerative disorders related to dementia. J Nucl Med Off Publ Soc Nucl Med 51:1418–1430
3. Furumoto S, Okamura N, Iwata R, Yanai K, Arai H, Kudo Y (2007) Recent advances in the development of amyloid imaging agents. Curr Top Med Chem 7:1773–1789
4. Okamura N, Fodero-Tavoletti MT, Kudo Y et al (2009) Advances in molecular imaging for the diagnosis of dementia. Expert Opin Med Diagn 3:705–716
5. Klunk WE, Engler H, Nordberg A et al (2004) Imaging brain amyloid in Alzheimer's disease with Pittsburgh Compound-B. Ann Neurol 55:306–319
6. Vandenberghe R, Van Laere K, Ivanoiu A et al (2010) ^{18}F-flutemetamol amyloid imaging in Alzheimer disease and mild cognitive impairment: a phase 2 trial. Ann Neurol 68:319–329
7. Barthel H, Gertz HJ, Dresel S et al (2011) Cerebral amyloid-beta PET with florbetaben (^{18}F) in patients with Alzheimer's disease and healthy controls: a multicentre phase 2 diagnostic study. Lancet Neurol 10:424–435
8. Clark CM, Schneider JA, Bedell BJ et al (2011) Use of florbetapir-PET for imaging beta-amyloid pathology. Jama 305:275–283
9. Jureus A, Swahn BM, Sandell J et al (2010) Characterization of AZD4694, a novel fluorinated Abeta plaque neuroimaging PET radioligand. J Neurochem 114:784–794
10. Rowe CC, Ng S, Ackermann U et al (2007) Imaging beta-amyloid burden in aging and dementia. Neurology 68:1718–1725
11. Hatashita S, Yamasaki H (2010) Clinically different stages of Alzheimer's disease associated by amyloid deposition with [^{11}C]-PIB PET imaging. J Alzheimer's Dis JAD 21:995–1003
12. Villemagne VL, Pike KE, Chetelat G et al (2011) Longitudinal assessment of Abeta and cognition in aging and Alzheimer disease. Ann Neurol 69:181–192
13. Dickson TC, Vickers JC (2001) The morphological phenotype of beta-amyloid plaques and associated neuritic changes in Alzheimer's disease. Neuroscience 105:99–107
14. Okamura N, Suemoto T, Shimadzu H et al (2004) Styrylbenzoxazole derivatives for *in vivo* imaging of amyloid plaques in the brain. J Neurosci 24:2535–2541
15. Kudo Y, Okamura N, Furumoto S et al (2007) 2-(2-[2-Dimethylaminothiazol-5-yl]ethenyl)-6- (2-[fluoro]ethoxy)benzoxazole: a novel PET agent for *in vivo* detection of dense amyloid plaques in Alzheimer's disease patients. J Nucl Med 48:553–561
16. Barthel H, Luthardt J, Becker G et al (2011) Individualized quantification of brain beta-amyloid burden: results of a proof of mechanism phase 0 florbetaben PET trial in patients with Alzheimer's disease and healthy controls. Eur J Nucl Med Mol Imaging 38:1702–1714
17. Waragai M, Okamura N, Furukawa K et al (2009) Comparison study of amyloid PET and voxel-based morphometry analysis in mild cognitive impairment and Alzheimer's disease. J Neurol Sci 285:100–108
18. Kudo Y, Furumoto S, Okamura N (2010) Benzoxazole derivatives. US Patent Application 2010/0021385
19. Shao H, Okamura N, Sugi K et al (2010) Voxel-based analysis of amyloid positron emission tomography probe [^{11}C]BF-227 uptake in mild cognitive impairment and Alzheimer's disease. Dement Geriatr Cogn Disord 30:101–111
20. McKhann G, Drachman D, Folstein M, Katzman R, Price D, Stadlan EM (1984) Clinical diagnosis of Alzheimer's disease: report of the NINCDS-ADRDA Work Group under the auspices of Department of Health and Human Services Task Force on Alzheimer's Disease. Neurology 34:939–944
21. Petersen RC, Smith GE, Waring SC, Ivnik RJ, Tangalos EG, Kokmen E (1999) Mild cognitive impairment: clinical characterization and outcome. Arch Neurol 56:303–308
22. Okamura N, Shiga Y, Furumoto S et al (2009) *In vivo* detection of prion amyloid plaques using [^{11}C]BF-227 PET. Eur J Nucl Med Mol Imaging 37:934–941
23. Kikuchi A, Takeda A, Okamura N et al (2010) *In vivo* visualization of alpha-synuclein deposition by carbon-11-labelled 2-[2-(2-dimethylaminothiazol-5-yl)ethenyl]-6-[2-(fluoro)ethoxy]benzoxazole positron emission tomography in multiple system atrophy. Brain J Neurol 133:1772–1778
24. Gauthier S, Reisberg B, Zaudig M et al (2006) Mild cognitive impairment. Lancet 367:1262–1270
25. Haroutunian V, Perl DP, Purohit DP et al (1998) Regional distribution of neuritic plaques in the nondemented elderly and subjects with very mild Alzheimer disease. Arch Neurol 55:1185–1191
26. Fodero-Tavoletti MT, Mulligan RS, Okamura N et al (2009) *In vitro* characterisation of BF227 binding to alpha-synuclein/Lewy bodies. Eur J Pharmacol 617:54–58
27. Fodero-Tavoletti MT, Smith DP, McLean CA et al (2007) *In vitro* characterization of Pittsburgh compound-B binding to Lewy bodies. J Neurosci Off J Soc Neurosci 27:10365–10371

Geriatrics Gerontology International — Medline Indexed

Geriatr Gerontol Int 2013; **13:** *215–221*

ORIGINAL ARTICLE: BIOLOGY

Brain accumulation of amyloid β protein visualized by positron emission tomography and BF-227 in Alzheimer's disease patients with or without diabetes mellitus

Naoki Tomita,[1] Katsutoshi Furukawa,[1] Nobuyuki Okamura,[3] Manabu Tashiro,[4] Kaori Une,[1] Shozo Furumoto,[3] Ren Iwata,[5] Kazuhiko Yanai,[3] Yukitsuka Kudo[2] and Hiroyuki Arai[1]

[1]Department of Geriatrics and Gerontology, Division of Brain Sciences, Institute of Development, Aging and Cancer, [2]Department of NeuroImaging Research, Innovation New Biomedical Engineering Center, Tohoku University, [3]Department of Pharmacology, Tohoku University Graduate School of Medicine, [4]Division of Cyclotron Nuclear Medicine, and [5]Division of Radiopharmaceutical Chemistry, Cyclotron and Radioisotope Center, Sendai, Miyagi, Japan

Aim: Although diabetes mellitus (DM) is considered to be one of the most consistent risks for developing dementia, it is not known if the pathology in dementia patients with DM is similar to or distinct from typical pathological features of Alzheimer's disease (AD). To discover the mechanism of developing dementia in AD patients with DM in a living state, we studied the distribution of amyloid β (Aβ) protein of diabetic AD patients.

Methods: To evaluate the accumulation of Aβ, we examined 14 normal controls, four diabetic patients with AD and 11 non-diabetic patients with AD by positron emission tomography (PET) using BF-227, a currently developed Aβ tracer.

Results: The analysis of PET images among the three groups showed an abundant aggregated Aβ accumulation in the cerebral cortex of both AD patients with and without DM. The extent and distributions of BF-227 accumulation in diabetic AD patients were not significantly different from these of non-diabetic AD patients.

Conclusion: These results suggest that the degree and extent of Aβ deposition is not significantly different between AD with DM and AD alone. **Geriatr Gerontol Int 2013; 13: 215–221.**

Keywords: Alzheimer's disease, amyloid β-peptides, diabetes mellitus, positron emission tomography.

Introduction

Long-standing lifestyle-related disorders from midlife, such as diabetes mellitus (DM) and hypertension, as well as obesity, are likely to be prominent risk factors for developing dementia and Alzheimer's disease (AD).[1] In fact, it is often found that diabetic patients develop AD in their later stage of life. Several separate community-based studies suggest that DM might increase the risk of dementia and AD,[2] though the underlying mechanisms are still not clearly explained.

Accepted for publication 9 April 2012.

Correspondence: Professor Hiroyuki Arai MD PhD, Department of Geriatrics and Gerontology, Division of Brain Sciences, Institute of Development, Aging and Cancer, Tohoku University, 4-1 Seiryomachi, Aobaku, Sendai 980-8498, Japan. Email: harai@idac.tohoku.ac.jp

AD is well characterized by an accumulation of misfolded proteins in the aging brain, which results in oxidative and inflammatory damage that in turn leads to energy failure and synaptic dysfunction.[3] In contrast, the impact of DM on the central nervous system (CNS) is not clearly understood.

Three major components related to type 2 DM that might underlie the effect of diabetes on the CNS in the development of AD are insulin resistance, hyperinsulinemia and hyperglycemia.[4] In addition to these three components, several other components are associated with the incidence of dementia or progression of cognitive decline. Whitmer *et al.* reported that severe hypoglycemic events were associated with a greater risk of dementia.[5] In addition, daily acute glucose fluctuations are also reported to be associated with cognitive decline.[6] Leptin, adiponectin and glucagon like peptide-1 (GLP-1) have recently been mentioned as potential factors that

doi: 10.1111/j.1447-0594.2012.00880.x

are associated with the development of AD.[7–10] These components are not fully independent of each other, and it is unlikely that the impact of DM on the CNS depends exclusively on a single component. Which components play the major role might depend on the patient's clinical history and the present state of DM.

Each of these components are thought to act on several different pathways that are important in the pathophysiology of AD, either indirectly, through inflammation or the development of vascular disease, or directly, through effects on amyloid and tau metabolism, and the formation of advanced glycation end-products (AGE).[11] (Fig. 1)

Autopsy results in an epidemiological study concluded that macroscopic brain infarcts are more common in people with DM than those without the disorder, as well as microvascular changes.[12] In contrast, the reported incidence of Alzheimer's pathology in the brains of people with diabetes varies between studies. There are several contradictory papers reporting the relationship between DM and AD. Beeri *et al.* have reported that type 2 DM is inversely associated with AD pathology; that is, diabetic patients with dementia have a significantly lower density of senile plaques than non-diabetic patients with dementia.[13] Matsuzaki *et al.* reported that hyperinsulinemia and hyperglycemia caused by insulin resistance are positively associated with the pathology of AD.[14] In the autopsy population of the Honolulu-Asia Aging Study, the occurrence of neurofibrillary tangles and amyloid plaques in the hippocampus and cortex in people without the apolipoprotein E (*APOE*) ε4 allele were similar to those with and without DM. However, as for *APOE* ε4 carriers, these lesions were more common in people with DM than in people without DM.[12] It was also reported that DM is related to generating atherosclerosis and cerebral infarction, but not directly to AD pathology in diabetic patients with dementia.[15,16] Autopsy findings are usually a mixture of many changes occurring during the living state, so the findings do not necessarily reflect the changes that are clinically relevant.

Interaction between medication for DM, especially the effect of insulin use, and AD neuropathology should be considered as well, as the population of insulin users showed a much higher risk of developing dementia in a cohort study.[17] Biessels *et al.* showed significantly fewer amyloid plaques in diabetic patients who received both insulin and oral antidiabetic medication, as compared with diabetic patients with other medication statuses or non-diabetic subjects. The effects of diabetes medication were specific to amyloid plaques, as the extent of neurofibrillary tangles pathology was not associated with diabetes medications.[18] However, these findings are derived from autopsies, and it is not certain if the same results can be gained from living human brains.

Several neuroimaging studies reported that DM is a risk factor for silent and symptomatic brain infarcts seen with magnetic resonance imaging (MRI),[19,20] and DM is also associated with cortical and subcortical atrophy.[21–23] As functional imaging, it is well known that reductions in regional cerebral glucose metabolic rate (CMRglu), as measured by fludeoxyglucose F 18 positron emission tomography (FDG-PET), are associated with increased AD risk and can be observed years before the onset of dementia.[24,25] Baker *et al.* reported that insulin resistance in persons with normal cognition and prediabetes or early diabetes without treatment is associated with reductions in CMRglu measured with FDG-PET.[26] However, previous radiological studies had limitations on discussing the pathological mechanism, as the modalities used were not directly linked to Alzheimer's pathology. No studies have been carried out regarding a pathobiological link between DM and AD in living human subjects.

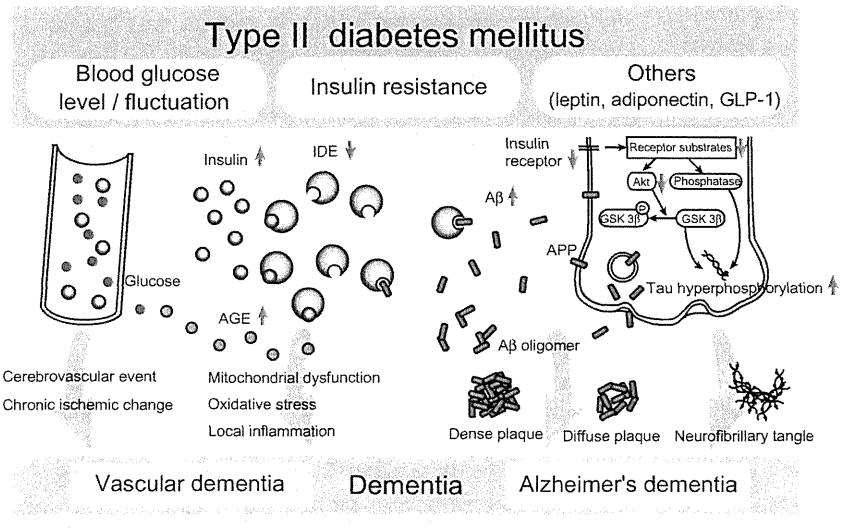

Figure 1 The possible pathological mechanisms associated with the impact of type 2 diabetes mellitus (DM) on the central nervous system (CNS). The major components of DM are described in the second column (only the three major components are described for easier understanding, though several other components are mentioned). Just below the column, the possible mechanism of developing dementia in type 2 DM. Aβ, amyloid β protein; AGE, advanced glycation end-products, APP, amyloid precursor protein; GLP-1, glucagon like peptide-1; GSK-3β, glycogen synthase kinase 3β; IDE, insulin degrading enzymes.

Table 1 Demographic data of the study participants

	Diagnostic group Normal control	AD alone	AD with DM
n	14	11	4
Sex (male/female)	7/7	4/7	2/2
Age	64.5 ± 2.9	78.5 ± 3.9	77.5 ± 5.2
MMSE	29.9 ± 0.1	20.5 ± 0.8	19.4 ± 2.8
ApoE ε4 allele (%)	0.12	0.35	0.37
HbA_{1c} (%)	5.7 ± 0.1	5.8 ± 0.1	7.2 ± 0.4

AD, Alzheimer's disease; DM, diabetes mellitus; HbA_{1c}, glycated hemoglobin; MMSE, Mini-Mental State Examination.

In order to clarify etiology and dementia subtypes in diabetic patients, we took a unique approach to visualize amyloid β protein (Aβ) deposition by positron emission tomography (PET) in living diabetic patients with dementia. The Aβ accumulation is successfully and non-invasively visualized by a recently-developed novel amyloid imaging probe called BF-227.[27–31] We used this tracer and applied it to "diabetic" and "non-diabetic" patients with clinically-diagnosed AD, to obtain more insights into differences in the extent and distribution of Aβ accumulation between diabetic and non-diabetic groups.

Methods

A total of 14 normal controls (NC), four diabetic patients with AD (AD with DM) and 11 non-diabetic patients with AD (AD alone) were examined. All the dementia patients were clinically diagnosed as probable AD according to the clinical criteria by "the National Institute of Neurological and Communicative Disorders and Stroke – Alzheimer's Disease and Related Disorders Association".[32] Brain MRI (1.5 Tesla; General Electric, Fairfield, CT, USA) was carried out on all the participants to exclude other causes of dementia. All the DM types of diabetic patients with AD were type 2. The study protocol was approved by the Committee on Clinical Investigation at Tohoku University School of Medicine and the Advisory Committee on Radioactive Substances at Tohoku University. After a complete description of the study to the patients and subjects, written informed consent was obtained.

The PET procedure using BF-227 is described elsewhere.[28,31] BF-227 and its *N*-desmethylated derivative (a precursor of [^{11}C]BF-227) were custom-synthesized by Tanabe R&D Service (Osaka, Japan) [^{11}C]BF-227 was synthesized from the precursor by *N*-methylation in dimethyl sulfoxide using [^{11}C]methyl triflate. The [^{11}C]BF-227 PET study was carried out using a PET SET-2400W scanner (Shimadzu, Kyoto, Japan). After intravenous injection of 211–366 mBq of [^{11}C]BF-227, dynamic PET images were obtained for 60 min with each subject's eyes closed. Standardized uptake value (SUV) images of [^{11}C]BF-227 were obtained by normalizing tissue radioactivity concentration by injected dose and bodyweight. Regions of interest (ROI) were placed on individual axial MR images in the cerebellar hemisphere, striatum, frontal, lateral temporal, medial temporal, parietal, occipital, anterior and posterior cingulate cortices. The ROI information was then copied onto dynamic PET SUV images, and regional SUV were sampled using Dr.View/LINUX software (AJS, Tokyo, Japan). Because there were neither senile plaques nor glucose hypometabolism in the cerebellum of AD patients, the ratios of regional SUV to cerebellar SUV (SUVR) were calculated as an index of [^{11}C]BF-227 retention. Neocortical SUVR was calculated by averaging SUVR in the frontal, lateral temporal, parietal and posterior cingulate cortices. Apolipoprotein E genotyping was carried out as previously described.[33]

The difference of Neocortex SUVR between the group of AD with DM and other groups was assessed with Student's *t*-test. The performance of diagnostic indices to discriminate among groups was assessed using receiver operating characteristic (ROC) analysis. Areas under ROC curves (AUC) were calculated and compared using GraphPad Prism Software (GraphPad Software, San Diego, CA, USA). Statistical significance was defined as $P < 0.05$.

Results

The clinical features of the three groups, NC, AD alone and AD with DM, are described in Table 1. Severities of dementia assessed by Mini-Mental State Examination were not significantly different between AD alone and AD with DM. Three patients were treated with only oral DM medications (patient A glimepiride + pioglitazone; patient B glimepiride + metformin + voglibose; patient

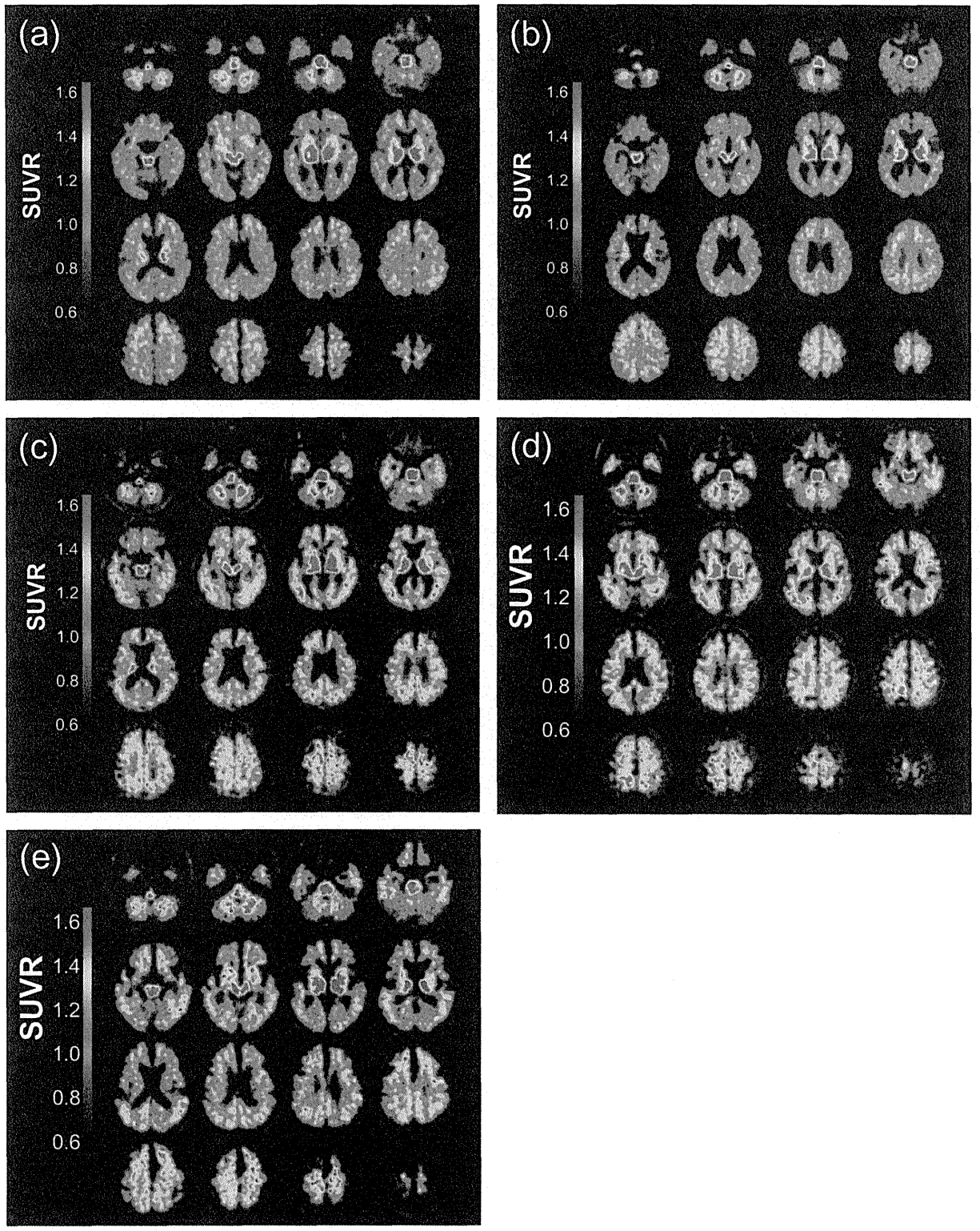

Figure 2 Representative BF-227 positron emission tomography images of each diagnostic group. (a) Normal control without diabetes mellitus (DM; 67-years-old, male, no complication; neocortical ratios of regional standardized uptake value to cerebellar standard uptake value ratio [SUVR] = 1.122). (b) Normal control with diabetes mellitus (67-years-old, female, insulin user; neocortical SUVR = 1.012). (c) Alzheimer's disease (AD) alone (75-years-old, female; neocortical SUVR = 1.230). (d) AD with DM (79-years-old, female, insulin user; neocortical SUVR = 1.240). (e) AD with DM (78-years-old, male, non-insulin user; SUVR = 1.18).

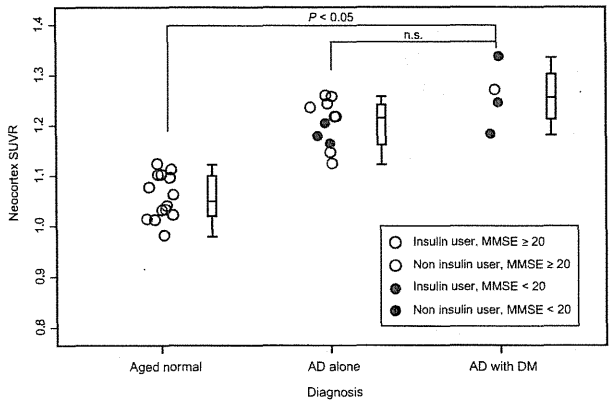

Figure 3 Box and scatter plots of ratios of regional standardized uptake value to cerebellar standard uptake value ration (SUVR) values with BF-227 in aged normal, Alzheimer's disease (AD) alone and AD with diabetes mellitus (DM) participants. Each circle indicates the mean SUVR from the mean neocortex. Red colored circle represents insulin user, whereas blue colored circle represents non-insulin user. There are no DM patients in the aged normal group shown with the blue circle. The filled circle represents the participants with Mini-Mental State Examination score less than 20. Although both AD with DM and AD alone showed significantly higher SUVR than the normal control group ($P < 0.05$), the difference between AD with DM and AD alone was not significant (n.s.).

Table 2 Characteristics of insulin users

	Subject 1 (no. 4) (normal cognition)	Subject 2 (no. 6) (AD patients)
Age	67	79
Sex	Female	Female
MMSE	28	21
ApoE genotype	3/3	3/3
CSF total tau (pg/ml)	–	334
BMI	24.7	19.8
HbA_{1c} (%)	7.6	8.2
Medication	Insulin only	Insulin, metformin
Hypoglycemic event	several	none
Duration of insulin use (years)	11	7

AD, Alzheimer's disease; BMI, body mass index; CSF, cerebrospinal fluid; HbA_{1c}, glycated hemoglobin; MMSE, Mini-Mental State Examination.

C metformin + voglibose), whereas only one AD with DM patient used insulin in addition to metformin. One DM patient was present in the normal control group. This patient in the control group had no oral medication. Insulin injection was the only medication.

MRI scans showed no or very few ischemic or hemorrhagic lesions observed in any of the participants. These small lesions were not strategic. White matter lesions (both periventricular and deep white matter) are all less than mild according to the Fazekas criteria (data not shown).[34]

After we obtained demographic information, we analyzed PET images with BF-227 among the three groups, and representative brain PET images are shown in Figure 2. As indicated in the figure, both the patients with AD alone and AD with DM showed significantly more robust retention of BF-227 than NC. Statistical analysis showed a significantly higher SUV-R of BF-227 ($P < 0.05$) in the cerebral cortex of AD alone and AD with DM than NC, as shown in Figure 3. Neocortical SUV-R of BF-227 in AD alone and AD with DM are not significantly different. Both the patients with AD alone and AD with DM showed increased BF-227 uptake in frontal, temporal, parietal, occipital and cingulated gyrus. The pattern of uptake was similar between the DM patients with insulin use and those without the use of insulin (Fig. 2). A similar pattern of uptake between insulin users and non-insulin users was seen both in the control group and the AD with DM group.

The clinical profiles of the two insulin users are shown in Table 2.

Discussion

The present study had two major findings. First, the uptake of BF-227 was significantly higher in both AD groups than that of the normal control group, regardless of DM complication. Second, the amount and pattern of the uptake was not affected by the use of insulin, both in the control group and the AD with DM group.

The first result that the severity and extent of the deposition did not differ significantly between the two groups suggests that both AD with DM and AD alone have robust deposition of senile plaques or typical AD pathology. In addition, all the participants we examined showed no or very few vascular lesions observed with MRI, indicating that we could exclude vascular dementia. The present result showed that the cause of developing dementia in DM patients cannot be fully explained by vascular mechanism. From the results of previous studies,[13,14] we assumed that either extra or less deposition of amyloid plaques would be seen in the brain of AD patients with DM complication. However, the brains of AD patients with DM showed a similar pattern and severity of the amyloid deposition to that seen in the brains of AD without DM complication. One possible explanation is that some kinds of protein that cannot be detected by BF-227 play a more important role than the classical aggregated plaque. Soluble

Aβ oligomers, which cannot be detected by BF-227, were shown to lower insulin receptor responses to insulin and cause substantial loss of neuronal surface insulin receptors.[35] Another possibility is that the additional effect of DM complication appears mainly through the increase in phosphorylation of tau, instead of an increase of Aβ plaque.

The second result of AD patients is in conflict with those reported by Beeri *et al.*[18] According to their conclusion, the AD patient with insulin and metformin use (subject 4 in Fig. 2) should have shown fewer senile plaques (lower uptake) as compared with diabetic patients with other medication status or non-diabetic subjects. One explanation for this inconsistency is that he/she was an *APOE* ε4 non-carrier. The occurrence of neurofibrillary tangles and amyloid plaques in people without the *APOE* ε4 allele were similar to those with and without DM in the autopsy population of the Honolulu-Asia Aging Study.[12] It is assumed that the effect of insulin and other medication use on reducing the plaques might only be effective in reducing the extra deposition of amyloid plaques in *APOE* ε4 carriers.

It was also found that the insulin user with normal cognition (subject 2 in Fig. 2) showed no difference in uptake. This subject was not obese, and started insulin injections 11 years before she undertook the PET procedure. Her glycohemoglobin level was 7.6%, and she had experienced several hypoglycemic events just before participation in the present study. From these clinical features, we assume that one of the main components of her DM were fluctuations of her blood glucose level (hyperglycemia and hypoglycemia). The interaction with ApoE ε4 might also be thought to be an explanation.

A limitation of the present study was that we could not adjust some factors, such as age, due to the small sample size. Because of the small sample size, the present study should be treated as a preliminary report. In addition, we could not measure the value of their homeostasis model assessment ratio, which is one of the key indicators of insulin resistance. We could not measure this indicator of insulin users, because they already had started insulin before admission to our clinic. Further studies are required to clarify the present report.

In conclusion, the present study provided new and important preliminary findings that a similar pathomechanism, which is the deposition of robust aggregated Aβ in the brain, is shared in both AD with DM and AD alone.

Disclosure statement

The authors declare no conflict of interest.

References

1 Barnes DE, Yaffe K. The projected effect of risk factor reduction on Alzheimer's disease prevalence. *Lancet Neurol* 2011; **10**: 819–828.
2 Biessels GJ, Staekenborg S, Brunner E, Brayne C, Scheltens P. Risk of dementia in diabetes mellitus: a systematic review. *Lancet Neurol* 2006; **5**: 64–74.
3 Querfurth HW, LaFerla FM. Alzheimer's disease. *N Engl J Med* 2010; **362**: 329–344.
4 Schrijvers EM, Witteman JC, Sijbrands EJ, Hofman A, Koudstaal PJ, Breteler MM. Insulin metabolism and the risk of Alzheimer disease: the Rotterdam Study. *Neurology* 2010; **75**: 1982–1987.
5 Whitmer RA, Karter AJ, Yaffe K, Quesenberry CP Jr, Selby JV. Hypoglycemic episodes and risk of dementia in older patients with type 2 diabetes mellitus. *JAMA* 2009; **301**: 1565–1572.
6 Rizzo MR, Marfella R, Barbieri M *et al.* Relationships between daily acute glucose fluctuations and cognitive performance among aged type 2 diabetic patients. *Diabetes Care* 2010; **33**: 2169–2174.
7 Wrighten SA, Piroli GG, Grillo CA, Reagan LP. A look inside the diabetic brain: contributors to diabetes-induced brain aging. *Biochim Biophys Acta* 2009; **1792**: 444–453.
8 Luchsinger JA. Diabetes, related conditions, and dementia. *J Neurol Sci* 2010; **299**: 35–38.
9 McClean PL, Parthsarathy V, Faivre E, Holscher C. The diabetes drug liraglutide prevents degenerative processes in a mouse model of Alzheimer's disease. *J Neurosci Nurs* 2011; **31**: 6587–6594.
10 Une K, Takei YA, Tomita N *et al.* Adiponectin in plasma and cerebrospinal fluid in MCI and Alzheimer's disease. *Eur J Neurol* 2011; **18**: 1006–1009.
11 Sims-Robinson C, Kim B, Rosko A, Feldman EL. How does diabetes accelerate Alzheimer disease pathology? *Nat Rev Neurol* 2010; **6**: 551–559.
12 Peila R, Rodriguez BL, Launer LJ. Type 2 diabetes, APOE gene, and the risk for dementia and related pathologies: the Honolulu-Asia Aging Study. *Diabetes* 2002; **51**: 1256–1262.
13 Beeri MS, Silverman JM, Davis KL *et al.* Type 2 diabetes is negatively associated with Alzheimer's disease neuropathology. *J Gerontol A Biol Sci Med Sci* 2005; **60**: 471–475.
14 Matsuzaki T, Sasaki K, Tanizaki Y *et al.* Insulin resistance is associated with the pathology of Alzheimer disease: the Hisayama study. *Neurology* 2010; **75**: 764–770.
15 Arvanitakis Z, Schneider JA, Wilson RS *et al.* Diabetes is related to cerebral infarction but not to AD pathology in older persons. *Neurology* 2006; **67**: 1960–1965.
16 Ahtiluoto S, Polvikoski T, Peltonen M *et al.* Diabetes, Alzheimer disease, and vascular dementia: a population-based neuropathologic study. *Neurology* 2010; **75**: 1195–1202.
17 Ott A, Stolk RP, van Harskamp F, Pols HA, Hofman A, Breteler MM. Diabetes mellitus and the risk of dementia: the Rotterdam Study. *Neurology* 1999; **53**: 1937–1942.
18 Beeri MS, Schmeidler J, Silverman JM *et al.* Insulin in combination with other diabetes medication is associated with less Alzheimer neuropathology. *Neurology* 2008; **71**: 750–757.
19 Longstreth WT Jr, Bernick C, Manolio TA, Bryan N, Jungreis CA, Price TR. Lacunar infarcts defined by magnetic